THE UNIVERSITY OF ALBERTA

SOLUTE SEGREGATION TO FREE SURFACES

IN IRON

by

Ⓒ   J.T. GRAY

A THESIS

SUBMITTED TO THE FACULTY OF GRADUATE STUDIES AND RESEARCH

IN PARTIAL FULFILMENT OF THE REQUIREMENTS FOR THE DEGREE OF

MASTER OF SCIENCE IN METALLURGICAL ENGINEERING

DEPARTMENT OF MINING AND METALLURGY

EDMONTON, ALBERTA

SPRING, 1972

THE UNIVERSITY OF ALBERTA

FACULTY OF GRADUATE STUDIES AND RESEARCH

The undersigned certify that they have read, and recommend to the

Faculty of Graduate Studies and Research for acceptance, a thesis

entitled Solute Segregation to Free Surfaces in Iron submitted by

J.T. Gray in partial fulfilment of the requirements for the degree of

Master of Science.

Abstract

Manganese and nickel were alloyed with iron together and individually. It was found that nickel does not segregate to free surfaces while manganese does and that the segregation of manganese is diffusion controlled. Manganese segregates into a region approximately one micron deep, the solute concentration in this region increasing by about 200%. This effect is believed to be real and not associated with oxide formation, inclusions or second phase precipitation. Several possible models which might explain the increase in manganese concentration in the free surface region are discussed and rejected. There are no interaction effects when manganese and nickel are both present in an iron specimen.

Acknowledgements

The author thanks Dr. M.L. Wayman and Dr. F.H. Vitovec for their help throughout the project.

Thanks also go to G. Chaisson for construction of the experimental equipment, T. Forman for help with the electronics and to R. Scott for assistance with the photography and metallography.

The author is indebted to D. Tomlinson and R. McDougal, operators of the electron microprobe.

TABLE OF CONTENTS

List of Tables

List of Figures

List of Appendices

1. Introduction

Segregation to free surfaces is obviously important since metal surfaces are directly exposed to environments in which they are used. Despite this importance very little work has been done in this area. However, segregation to internal surfaces (grain boundaries) has been studied by a number of workers. Their results are reviewed below.

1.1 Characteristics of Segregation to Grain Boundaries

Segregation to internal surfaces under non-equilibrium conditions has in the past been studied indirectly by measuring changes in physical properties and directly by quantitatively measuring the solute content.

1.1.1 Indirect Evidence of Segregation to Grain Boundaries

Grain boundary hardening has been used to measure segregation indirectly. Westbrook et al (1) and Aust (2,3) have studied boundary hardening as a function of segregation using a microhardness tester. Indentations were made on a traverse oblique to the grain boundary. Following is a list of the characteristics of the hardening phenomenon.

1. Grain boundary regions of high purity metals are softer than regions away from the grain boundary. Figure 1 is a hardness profile across a grain boundary of a high purity metal. A soft grain boundary region has been observed in high purity zinc (2) and in high purity lead (1). Hardness differences between grains are due to orientation.

2. Additions of solute atoms cause an increase in the hardness of the boundary relative to the grain. Figure 2 is of such a solvent-solute system. Grain boundary hardening has been observed in the Pb-Au, Pb-Ag, Pb-In (1), Zn-Al, Sn-Pb, Pb-In,

Pb-Sn, Pb-Ag and Pb-Au (2) systems.

3. A specific heat treatment is involved in producing grain boundary hardening. Aust et al (2) produced hardening in zinc, lead and tin systems by a high temperature anneal followed by an air quench to room temperature.

4. While some solute additions produce increases in grain boundary hardness, others leave the hardness unaffected, as in the high purity metal with no solute additions. Aust et al (2) alloyed 100 ppm gold with zinc and 50 ppm antimony with tin. In both cases the effect is a soft grain boundary region, identical to that of the metal without any alloy additions. Variations in antimony content in the tin-antimony system from 10 to 50 ppm do not change the hardness of the boundary region.

5. Substantial grain boundary hardening can arise from very small solute additions. However, past a certain limit hardening increases at a much slower rate. Floreen (4) found that the grain boundary hardness of nickel samples increases markedly with an increase in sulfur content from 10 to 100 ppm. Similarly, Westbrook et al (1) observed that an addition of 0.04 ppm gold to lead results in 10% excess hardening at the grain boundary over that of the grain. Beyond 0.2 ppm gold the excess hardening increases at a much slower rate. Aust et al (2) found that lead added to tin produces grain boundary hardening, however beyond 20 ppm lead, grain boundary hardness remains constant.

6. Grain interior hardness does not increase measurably with relatively

large amounts of solute. Aust et al (2) found that the bulk grain hardness of a lead-tin alloy is not affected by solute additions of 0 to 50 ppm tin. Similarly, Floreen (4) observed sulfur additions between 0 and 100 ppm do not affect the bulk grain hardness of nickel-sulfur alloys.

7. The width of the region effected is not confined to the grain boundary itself but occurs over a rather wide region of the order of many microns in the vicinity of the grain boundary. Aust et al (3) found the region affected by hardening in a lead-1.3 ppm gold alloy to be approximately 250 microns wide on either side of the boundary (2). The width of hardened regions has also been measured from 10 to 40 microns and always exceeds the width of the grain boundary.

8. The solute is believed to remain in solid solution in the boundary region without forming any second phases. Past workers believed the hardening and softening of the boundaries to be caused by solute segregation either to or away from boundaries. None believed or found evidence for the formation of second phases.

9. An interaction effect between solutes exists. Boundary hardening associated with one solute can be removed by the addition of a suitable second solute. Sulfur (10 to 100 ppm) added to nickel produces grain boundary hardening (4). Adding 730 ppm magnesium to a nickel - 30 ppm sulfur alloys reduces grain boundary hardenss to that of pure nickel. Similarly, gold in lead causes grain boundary hardening while calcium in lead causes softening but when alloyed together in lead produce no boundary hardening.

10. The size difference between solute and solvent atoms is not a dominant factor in determining the presence of grain boundary hardening. Table 1 shows there is no correlation between solute-solvent atom size difference and grain boundary hardening.

11. There is a correlation between grain boundary hardening and the distribution coefficient. There is an inverse relationship between the relative effect of solute additions on boundary hardening and the distribution coefficient. Table 1 also shows grain boundary hardening always occurs with k (distribution coefficient) less than one and softening with k greater than one. Gold causes relatively greater boundary hardening in lead than indium in lead. It is found gold has a smaller distribution coefficient in lead than does indium (1).

12. Non-equilibrium grain boundary hardening occurs under the following conditions;

    (1) a positive vacancy-impurity binding energy, greater than kT.

    (2) solute atoms more mobile than solvent atoms. Hanneman and Anthony (5) proposed the following relation between the distribution coefficient (k), the diffusivity of the solvent (DA) and the diffusivity of the solute (DB);

    $$\ell n \ (DB/DA) \sim C \ (1-k)$$

    where C is a constant approximately equal to 3 at $1000^{\circ}k$. Thus, if k is less than one, then DB/DA is much greater than one and if k is greater than one, then DB/DA is much less than one. This means that solute atoms are more mobile than solvent atoms when k is less than one (grain boundary hardening).

A relationship has been found between k and the vacancy-
solute binding energy (B) for several different solutes
in a common solvent (2). Figure 3 shows B is always
positive but increases rapidly as k decreases. If k is
less than one, the binding energy between solute atoms
and vacancies is strongly positive and greater than kT,
the thermal energy of the alloy.

13. There is a correlation between positive deviations from
thermodynamic ideality and the presence of grain boundary
hardening. Table 2 shows that in every case where grain
boundary hardening occurs the activity coefficient of the solute
is greater than one. In those cases in which boundary hardening
does not occur the activity coefficient is less than one.

14. The effect of gold, silver, tin and indium on grain boundary
hardening of lead has been studied (1). Additions of gold less
than 0.02 ppm, silver less than 0.06 ppm, tin less than 2 ppm
and indium less than 40 ppm cause no grain boundary hardening.
There is a correlation between this effect and the distribution
coefficient. (Table 3). The smaller the distribution
coefficient (the lower the solubility of solute in solvent) the
more effective is the solute in producing grain boundary
hardening. Therefore, the smaller the distribution coefficient
the lower the solute concentration at which hardening is
observed. Figure 4 shows that solutes with smaller distribution
coefficients also cause greater increases in grain boundary
hardening per unit solute concentration.

15. Grain boundary hardness increases very rapidly with increasing

annealing temperature. Figure 5 shows that grain boundary hardness increases with increasing annealing temperature, while the grain hardness remains constant.

16. The rate at which a specimen is brought to room temperature determines the peak hardness values of grain boundaries and the width of the affected region. Figure 6 shows the faster the cooling rate, the higher and narrower the hardness peak, while the slower the cooling rate, the wider is the affected region.

17. The hardness of grain interiors and grain boundaries of dilute alloys is temperature dependent. Hardness profiles across grain boundaries determined at test temperature are shown in Figures 7, 8 and 9. It is shown that in the systems containing high solubility solutes, tin and indium, excess boundary hardness is retained at low temperatures but decreases as the temperature is raised. The excess hardening observed when the low solubility solutes, gold and silver, are present is lost at low and high temperatures.

18. Following an anneal and a quench, the grain boundary hardness is a function of holding time at the low temperature. Westbrook et al (1) found that grain boundary hardness may increase, decrease or remain constant with time. The boundary hardness appears to be dependent upon the alloy system and the temperature of the high and low temperature anneals.

1.1.2 Direct Evidence of Segregation to Grain Boundaries

Bercovici et al (6) measured segregation to grain boundaries by producing on his specimens a surface layer resistant to attack by dilute nitric acid. This surface layer was only defective at grain

boundaries. The grain boundaries of samples were thus etched and the solution was analyzed for solute by atomic absorption spectrometry. Following is a list of the characteristics of solute segregation to grain boundaries determined from direct measurements.

1. The solute concentration at grain boundaries following a high temperature anneal and a quench to room temperature is a function of the annealing temperature. A zinc – 0.1% cadmium alloy was held at different elevated temperatures and cooled to room temperature (6). Figure 10 shows there is a large increase in solute concentration at grain boundaries with increasing annealing temperature.

2. The solute concentration of a grain boundary following a high temperature anneal is a function of the cooling rate. Table 4 indicates that the solute concentration of a grain boundary following a water quench to room temperature is much less than a sample cooled at a slower rate.

3. Bercovici's (6) direct measurements of grain boundary segregation indicate that it is too great to be caused by equilibrium grain boundary segregation. Bercovici et al (6) found that the excess solute was equivalent to a 60 angstrom thick boundary layer of pure cadmium.

4. There is a correlation between excess solute present along grain boundaries and the distribution coefficient. The distribution coefficient for 0.1% cadmium in zinc is 0.2 (6). Segregation is evident when the distribution coefficient of the solute is less

than one.

5. There is a correlation between excess solute present along grain boundaries and the activity coefficient. The activity coefficient of 0.1% cadmium in zinc is between 3.162 and 4.611 (7). Segregation to grain boundaries occurs when the activity coefficient is greater than one.

1.2 Characteristics of Segregation Related Phenomena

1.2.1 Temper Brittleness

Temper brittleness occurs in certain steels when they are held within or cooled slowly through a particular temperature range. The brittleness can be revealed by a notch bar impact test at or below room temperature. This phenomenon occurs in alloy steels tempered between 350° and $525^{\circ}C$ or slowly cooled through this temperature range.

Low et al (8) used the following embrittling treatment;

(1) $593^{\circ}C$, 1 hour

(2) furnace cool to $538^{\circ}C$, hold 15 hours

(3) cool to $524^{\circ}C$, hold 24 hours

(4) cool to $496^{\circ}C$, hold 48 hours

(5) cool to $468^{\circ}C$, hold 72 hours

(6) cool to $315^{\circ}C$, air cool to room temperature.

The steel in this case contained 0.3 to 0.4% carbon, 3.5% nickel and 1.7% chromium. Temper brittleness was studied after adding approximately 500 ppm of several impurities (antimony, arsenic, phosphorous and tin). The characteristics of temper brittleness are listed below.

1. Embrittlement is completely reversible. Embrittlement is removed by a one hour anneal at $650^{\circ}C$ followed by a water quench to room temperature.

2. The fracture of non-embrittled specimens is transcrystalline while those of embrittled specimens is intercrystalline. There appears to be a grain boundary effect in the embrittled condition.

3. Embrittlement occurs in alloy steels when specific impurities (antimony, arsenic and tin) are present, but does not occur in the absence of these impurities.

4. Plain carbon steels are not embrittled even when a large amount of an impurity which embrittles alloy steels is present.

5. No second phase precipitate has been detected at the grain boundaries in embrittled steels.

6. Grain boundary hardening occurs in embrittled steels. The grain boundaries of embrittled steels are detectably harder than the matrix while the grain boundaries of non-embrittled or de-embrittled steels are softer than the matrix.

7. High purity alloy steels are not susceptible to temper embrittlement.

1.2.2 Intergranular Corrosion

Intergranular corrosion is a localized attack at the grain boundaries of a metal. The grain boundary acts as an anode and the grain interior acts as a cathode. Catastropic failure may result. Hanneman et al (5) discusses intergranular corrosion in zinc - 4% aluminum alloys and its characteristics are listed below.

1. There is a correlation between those solutes which cause an alloy to be susceptible to intergranular corrosion and the distribution coefficient. Additions of lead, tin and cadmium result in intergranular corrosion of zinc - 4% aluminum alloys (9) Table 5 shows that all three have a distribution coefficient less than unity.

2. There is a correlation between those solutes which cause an
    alloy to be susceptible to intergranular corrosion and the
    activity coefficient. The activity coefficients of lead, tin
    and cadmium in zinc are all greater than one (7).

3. There is an interaction effect between solutes. Additions of
    copper increase the permissable content of harmful impurities
    (lead, tin and cadmium) in zinc - 4% aluminum (9).

4. Additions of certain solute atoms cause an increase in the
    hardness of the boundary relative to the grain. Lead, tin and
    cadmium which cause susceptibility to intergranular corrosion,
    also cause grain boundary hardening in zinc - 4% aluminum (9).
    Copper added to zinc - 4% aluminum does not increase the
    boundary hardness relative to the grain.

1.3 Discussion

Temper brittleness, intergranular corrosion and segregation to
grain boundaries have several characteristics in common. Following is
a list of the characteristics held in common.

1. Grain boundary hardening is apparent in all three cases. As the
    solute concentration of certain alloy systems increases the grain
    boundary hardness also increases. Similarly, grain boundary
    hardening is detected in specimens susceptible to intergranular
    corrosion and temper embrittled materials.

2. In all three cases an interaction effect between solute elements
    is observed. Grain boundary hardening, intergranular corrosion
    and temper brittleness caused by the presence of a specific
    solute can be removed by the addition of a suitable second solute.

3. The effect of the solute can be observed at very low concentrations.

An average of only 10 to 500 ppm of solute is required to observe the desired effect.

4.   There is a correlation of solutes which cause grain boundary hardening, intergranular corrosion, and temper brittleness with the distribution and activity coefficients. Solutes with a distribution coefficient less than one and an activity coefficient greater than one are associated with the effects.

5.   Grain boundary hardening, intergranular corrosion and temper brittleness result following a specific heat treatment. The effect is observed following a high temperature anneal and return to room temperature.

The cause of grain boundary hardening, intergranular corrosion and temper brittleness is believed to be a high solute concentration in the grain boundary region. Since there has been very little investigation into the non-equilibrium segregation of solute to free surfaces and even less investigation under equilibrium conditions the purpose of this research is to study the segregation of manganese and nickel to free surfaces in iron in an attempt to evaluate the following variables;

1.   segregation as a function of time held at the high temperature anneal

2.   segregation as function of annealing temperature

3.   segregation as a function of cooling rate

4.   interaction effects of solutes.

2. Experimental Program and Procedures

2.1 Experimental Program

In order to study the segregation of manganese and nickel to free surfaces in iron the following experimental program was followed.

Series One.

Iron-manganese specimens were prepared and segregation was studied as a function of time held at the annealing temperature. All specimens had identical annealing temperature and cooling rate.

Series Two.

Segregation in iron-manganese samples was studied as a function of the annealing temperature, while the annealing time and cooling rate were constant.

Series Three.

In this case segregation effects in iron-manganese samples were studied as a function of cooling rate while the annealing temperature and time were kept constant.

Series Four.

Iron-manganese-nickel samples were prepared and interaction effects were studied as a function of cooling rate.

Series Five.

Iron-nickel samples were prepared and segregation was studied as a function of cooling rate.

Table 6 presents the experimental program in tabulated form.

The following sections describe the apparatus used and the techniques employed to obtain the results.

2.2 Description of Testing Apparatus

2.2.1 Electron Microprobe

The A.R.L. Electron Microprobe in the Department of Geology was
used in the analysis of some of the samples. Figure 11 is a block diagram
of the electron beam, x-ray system and pre-amplifier. Electrons bombard
the specimen. Flourescent x-rays are given off characteristic of the
elements present in the bombarded region of the sample. These x-rays
are detected by crystal spectrometers and the output enters a counting
circuit with a digital display (x-y chart recorder or typewriter
printout) and on a screen of a cathode ray tube for polaroid photography
(Figures 12, 13 and 14).

2.2.2 Electro-Sectioning Equipment

Equipment was designed and constructed to study segregation to free
surfaces on a scale finer than possible with the electron microprobe.
The principle of the electro-sectioning equipment (11) is to make the
specimen the anode in an electropolishing cell. The cathode is made
of metal and covered with filter paper impregnated with an electrolyte.
While current is flowing, the specimen is moved along the filter paper.
Material from the surface of the specimen is deposited along the
length of the filter paper in a continuous smear and a record of the
electrolytic current measures indirectly the amount of material removed.
The filter paper is then analyzed for solute. Figure 15 is a
schematic of this equipment. Chapters 2.3.1, 2.4.1 and Appendices 1
and 2 give a detailed account of the operation of the electro-sectioning
equipment.

2.2.3 Furnace

The samples were annealed in a Vycor tube placed inside a resistance box furnace. Temperature was measured with a chromel-alumel thermocouple and recorded with a Wheelco Temperature Controller. Maximum and minimum power to the furnace was controlled by two variacs.

A combination of gas flow, position of Vycor tube and power settings were used to control the cooling rate of a specimen from $1400^{\circ}F$ to room temperature. The specimen was quenched by sliding the Vycor tube out of the furnace until the specimen was visible and allowing a high flow of hydrogen to pass through the tube. The specimen reached room temperature in two to three minutes. A hydrogen cool was achieved in the same manner as the quench except that the hydrogen flow was not increased above the normal flow rate. Room temperature was reached in approximately three hours by turning off the power to the furnace and leaving the gas flow unchanged. Finally, step-cooling involved turning the power settings to successively lower values. The sample remained in the furnace and room temperature was reached in approximately five hours.

2.3 Specimen Preparation

2.3.1 Electro-Sectioning Specimen Preparation

Specimens were prepared in an arc furnace under an argon atmosphere from high purity iron, manganese and nickel (Appendix 3). The iron alloys were then reduced approximately 50% by rolling. Following this operation the alloys were roughly disc shaped, having a diameter of approximately 4.5 cm. and a thickness slightly greater than 1 cm. Using a copper tube and a Servomet Spark Machine cylindrical samples were removed from the discs. The cylindrical samples were machined to

0.7 cm. in height and 1.0 cm. in diameter. At this point the
samples were annealed for 72 hours at 1400°F in a hydrogen atmosphere
(99.99% minimum purity). Following this anneal, one end face of each
specimen was polished on successively finer grit ending with six
micron diamond paste. Next, each sample was reintroduced into the
furnace at the desired temperature for the required time in a hydrogen
atmosphere. These specimens were then electro-sectioned.

2.3.2 Electron Microprobe Specimen Preparation

Microprobe specimens were prepared from electro-sectioned samples.
The samples were cut once down the cylindrical axis and three times
perpendicular to the axis yielding eight microprobe specimens. These
specimens were half-moon shaped, approximately 0.9 cm. by 0.3 cm.
thick (Figure 16). Face B was mechanically polished perpendicular to
Face A to 6 micron diamond paste. Face A was polished to 600 grit.
Each specimen was introduced into the furnace separately for the desired
time and temperature. After removal from the furnace each specimen was
mounted in a one inch diameter bakelite mold (Figure 17) and polished
to 0.05 micron Linde B, carbon coated and tested in the electron
microprobe. Face B was contained within the bakelite and segregation
to this surface was studied.

2.4 Testing Procedure

2.4.1 Electro-Sectioning

The filter paper (Watman's #50 Acid Resisting Filter Paper) was
impregnated with an electrolyte composed of 765 ml. glacial acetic acid,
185 ml. perchloric acid and 50 ml. distilled water (12). Eight volts
were applied to the specimen from a constant voltage source. The
electro-sectioning was carried out in a temperature controlled glove

box between 4° and 8° C. The specimen rotated over the filter paper while the stainless steel cathode wheel with the filter paper attached revolved beneath the specimen. The polishing current passed through a one ohm resistor. The voltage across the resistor was recorded on a strip chart recorder moving at 0.2 inches/minute. The area under the chart paper therefore represented the number of ampere-seconds which had passed through the specimen. A calculation (Appendix 2) involving the number of ampere-seconds and the surface area of the specimen yielded the depth of material removed from the surface. By knowing the position of the specimen relative to the filter paper during electro-sectioning it was possible to calculate the depth of material removed on each increment of filter paper. The filter paper was then sectioned and dissolved in aqua regia. The solution was analyzed for manganese or nickel by atomic absorption spectrometry. This procedure yielded the solute concentration of each section of filter paper and further calculations (Appendix 2) yielded a graph of concentration of solute against depth below the surface.

2.4.2 Electron Microprobe

The first series of tests on the microprobe specimens involved the use of the x-y recorder, searching for nickel segregation. The electron beam was focused on the edge of the sample and moved inwards, perpendicular to the free surface. A graph of solute concentration against distance below the free surface was thus obtained. Another graph was obtained with the beam focused on the specimen at a depth several microns below the surface and traversed paralled to the surface. This revealed any changes in solute concentration at a constant distance below the free surface. None of these results were quantitative,

however they indicated whether a significant difference in solute concentration did exist.

The oscilloscope camera allowed polaroid pictures to be taken of the distribution of solute, as revealed by x-ray fluorescence, along the free surface and of the area directly beneath it. These pictures could be used semi-quantitatively by comparing the widths of regions showing solute segregation. Solute enriched zones appear as bright areas on the photographs.

Finally, quantitative results were obtained by comparing the number of counts from the samples with readings from standards.

3. Test Results

3.1 Segregation of Nickel

The x-y recorder of the electron microprobe was used to study the effect of cooling rate on nickel segregation. Specimens 5-1, 5-2 and 5-3 were tested. Each sample was searched for nickel segregation on a track from the free surface into the interior and also on a track parallel to the surface at various depths. Figure 18 shows the variation in nickel concentration with depth below the free surface and Figure 19 shows the variation in nickel concentration parallel to the free surface at a depth of five microns. Figures 18 and 19 were obtained from specimen 5-1 and are typical of all three samples. These two graphs show that there is no variation in nickel content with depth below or with distance parallel to the free surface. The apparent variation of nickel content with distance is within the scatter range of the probe.

Figure 20 is a photograph of sample 5-2 from the cathode ray tube of the electron microprobe. This shows an even distribution of nickel throughout the specimen.

Figure 21 is a graph showing the even distribution of nickel throughout sample 5-2 revealed by electro-sectioning. This graph is typical of results obtained by electro-sectioning other specimens in Series Five.

Summary

It appears that in an iron - 1.09% nickel alloy there is no detectable solute segregation to free surfaces at any of the cooling rates employed. The nickel appears to be evenly distributed throughout the material.

3.2 Segregation of Manganese

3.2.1 Segregation as a Function of Cooling Rate

Samples of Series 3A and 3B were used to study segregation as a function of cooling rate. Figure 22 is a photograph of sample 3B-1. Segregation of manganese to the free surface is barely distinguishable as small bright dots along the specimen-bakelite interface. A photograph of sample 3B-1 at a higher magnification (Figure 23) indicates clearly the segregation of manganese along the free surface. Breaks in the bright areas along the free surface in Figure 23 indicate the possibility of the segregation being discontinuous. Figure 24 confirms this.

Specimen 3B-2 is shown in Figures 25 and 26. Figure 25 shows the manganese to be segregated near the surface in a region much wider than that found in sample 3B-1 (Figure 23). However, Figure 26 which is a photograph of sample 3B-2 at a different location along the interface shows approximately the same degree of segregation as sample 3B-1 (Figure 23).

Figure 27 is a photograph of specimen 3B-3. The photograph shows the width of the high manganese region to be fairly constant, discontinuous and greater than the width of the high manganese region of sample 3B-1 (Figure 23).

Figures 28 to 30 are photographs of samples 3A-1, 3A-2 and 3A-4 respectively. These show the region of high manganese content of the step-cooled sample is approximately twice as wide as the quenched sample. However it can also be seen that the quenched sample has a wider manganese affected free surface region than the hydrogen cooled sample.

Summary

Within the range studied manganese segregates to free surfaces in iron. These regions are discontinuous and there appears to be no correlation between the cooling rate and the width of the high manganese region.

3.2.2 Segregation as a Function of Annealing Time

Experiments on samples 1-1 to 1-7 were conducted to study the effect of annealing time on manganese segregation. Plots of manganese concentration against depth below the free surface were made from electron microprobe measurements for all the specimens. The results were similar and are typified by Figures 30A and 31 from samples 1-2 and 1-5 respectively. Figure 32 is a plot of manganese concentration against depth below the free surface (sample 1-5) determined by the use of the electro-sectioning equipment. Figure 34 is a photograph of sample 1-7 and is typical of Series One specimens.

Figures 30A and 31 and the results obtained from the other samples of the same series have several features in common. The minimum manganese concentration occured at a depth of 5 microns below the surface. Between 5 and 10 microns a large increase in manganese concentration occured and at depths greater than 20 microns the concentration remained constant at the bulk alloy composition.

The electro-sectioning equipment was used to obtain the data shown in Figure 32. This and similar results from other specimens show a large manganese concentration near the surface. At a depth between five and ten microns the manganese concentration fell to its lowest level. Beyond ten microns the manganese concentration quickly increased to a relatively constant value which corresponded to the bulk alloy composition.

Both the electron microprobe and the electro-sectioning show that the minimum manganese concentration occurs between five and ten microns below the free surface. Beyond this depth the concentration increases rapidly to a relatively constant value.

Electron-microprobe results begin at a depth of five microns (Figures 30 and 31). The maximum concentration is found closer to the surface and is therefore observed only by electro-sectioning. Figure 32 shows that the solute concentration drops from its highest to lowest value between the free surface and a depth of seven microns. Thus the depleted zone exists when segregation occurs and in this case the probe shows only the depleted zone.

Manganese concentration against depth below the free surface was determined for sample 1-5 with both the electron microprobe and the electro-sectioning unit. Figure 33 reproduces the data from Figures 31 and 32. There is good agreement between the two experimental methods.

Figures 29 and 34 are photographs of samples 1-5 and 1-7 respectively. These figures show that the high manganese region remains discontinuous along the surface despite increases in annealing time. The photographs also show that the depth of this region is insensitive to annealing time at $1400^{\circ}F$.

Summary

It appears that following an anneal at $1400^{\circ}F$ manganese segregates to free surfaces in iron. The maximum manganese concentration occurs closest to the surface. The maximum concentration drops very rapidly and between five and ten microns below the surface a minimum solute concentration is reached. At depths greater than ten microns the manganese concentration increases to a constant value. With increasing

annealing time the width of the high manganese region does not increase nor does the segregation become continuous along the surface. Therefore, it appears the segregation of manganese to free surfaces in iron is not a function of annealing time.

3.2.3 Segregation as a Function of Annealing Temperature

Experiments on samples 2-1 to 2-7 were conducted to study the effect of annealing temperature at a constant annealing time of 24 hours on manganese segregation. Figure 35 is a photograph of sample 2-3. This sample was annealed at 1100°F and manganese segregation to the free surface is apparent. Figure 36 is a photograph of sample 2-7. This sample was annealed at 500°F and no manganese segregation to the free surface is evident. Figures 31, 37 and 38 are plots of manganese concentration against depth below the free surface taken on the electron microprobe for samples 2-1, 2-4 and 2-7 respectively. Figure 31 shows a low concentration of manganese at a depth of five microns corresponding to the segregation of solute to the free surface. Figures 37 and 38 show a relatively constant manganese concentration at all depths below the surface corresponding to an absence of solute segregation. Plots from specimens annealed at lower temperatures (2-5 to 2-7) appeared identical to Figures 37 and 38.

Summary

At or below 950°F manganese does not segregate to free surfaces in iron following a 24 hour anneal.

3.3 Interaction Effects

Figures 39 and 40 correspond to samples 4-1 and 4-2 respectively and are electron microprobe plots of the concentration of manganese and nickel against depth below the surface. Both figures show that the manganese concentration varies as a function of depth below the surface

while the nickel concentration remains constant. The low manganese values at a depth of five microns indicates manganese segregation to the free surface.

Summary

It appears there is no discernable interaction effect between manganese and nickel. The nickel solute behaves as if no manganese was present and the manganese behaves as if it were the only solute.

4. Discussion

This chapter will discuss the validity and compare the results of electron microprobe and electro-sectioning methods. Grain boundary segregation and manganese clustering will also be discussed. Following this, the segregation characteristics of manganese and nickel in iron will be discussed as well as the mechanisms postulated by others to explain this phenomenon.

4.1 Validity of Results

A certain statistical scatter is associated with each electron microprobe reading. This statistical scatter is about 7% of the readout value. Thus, for there to be a significant difference in solute concentration between two readings there must be at least a 7% difference between them. This scatter ($\pm7\%$) is marked on graphs determined with the use of the electron microprobe.

Analysis of material by the electro-sectioning method involves several steps and each introduces errors. To evaluate the accuracy of the final results the following procedure was adopted. The filter paper following an electro-sectioning experiment was analyzed in the normal manner (Appendix 1 and 2) and a graph of solute concentration against depth below the surface was drawn. Points distant from the surface (greater than thirty microns) were chosen which had equal areas under the voltage-time curve of the chart recorder. Assuming points very far from the surface have equal solute contents, the results from these points were compared. It was found that the solute concentration values of these regions were within a scatter range of $\pm10\%$ of the reading. Thus, there must be a difference greater than 10% between readings for there to be a significant difference in solute concentration. This

scatter (±10%) is marked on the graphs determined with the use of the electro-sectioning equipment.

The result of testing specimen 1-5 by both electron microprobe and electro-sectioning methods plotted in Figure 33 shows that there is good correlation between the two methods and both are capable of determining differences in solute concentration in the range studied.

It is possible that the high manganese concentration along the free surface is due to preferential manganese oxidation. There are several reasons why this is not believed to be the case. With increasing annealing time an oxide layer would be expected to increase in thickness whereas the thickness of the solute enriched zone is not a function of annealing time. In addition it is unlikely that an oxide layer would have a discontinuous nature unless some spalling off is occuring. However the oxide layer formed on heating these alloys in air is much thicker than a few microns and does not spall, thus there is no reason to expect a thin layer to spall. Finally, annealing was carried out in a high purity hydrogen atmosphere where oxidation should not occur.

It is possible that the discontinuous nature of the high manganese region could be a result of the polishing operation each specimen was subjected to between the anneal and the electron microprobe. This is not believed to be the case. Each sample was polished in one direction only. In approximately half the samples the polishing direction was perpendicular to the sample diameter (from the bakelite into the sample) and in the other half in a direction parallel to the sample diameter-bakelite interface. There is no correlation between the direction of the polishing and the discontinuous nature of the high manganese region.

Therefore, it is believed the increase in manganese concentration in the free surface region is not caused by oxide formation and the

discontinuous nature of the zone is believed to be real.

It is believed that the grinding and polishing operations employed before heat treatment do not influence the distribution of solute. After heat treatment, electro-sectioning and electron microprobe samples followed different experimental procedures. Both experimental techniques showed manganese segregation to free surfaces. Therefore the sample preparation techniques and the testing procedures, other than the heat treatment, are not believed to have an effect upon the solute distribution.

Testing by both methods indicates an increase in manganese concentration near the free surface. There is good correlation between results of the different techniques. Segregation is not an effect of the specimen preparation or testing procedures and is not a result of oxidation. Therefore, it is believed the segregation of manganese to the free surface is a real effect.

4.2 Grain Boundary Segregation

Figure 41 is an optical micrograph of microprobe sample 1-1. Similar micrographs were obtained from the other samples of this series and it was found that between 60 and 65 grain boundaries intersect the sample diameter (approximately 0.97 cm.). Therefore, the average distance between grain boundaries is from 149 to 161 microns. It would not be impossible therefore to photograph the surface with the electron microprobe at a high magnification (Figure 24) without a grain boundary being present in the field of view. However, it seems unlikely that a grain boundary would not be present in at least one of the lower magnification photographs (Figure 22). Therefore, in at least one of the photographs a grain boundary must be in the field of view. Manganese

segregation to free surfaces is shown by a bright band, yet in none

of the photographs is a grain boundary delineated by such a band.

Figure 22 shows segregation to the free surface faintly, yet nowhere

does there appear to be any such segregation along a grain boundary.

Thus, it appears that either segregation to grain boundaries does not

occur so that the grain interior and grain boundary have the same

solute content or else segregation either to or away from boundaries

occurs on a scale finer than the limit of resolution of the electron

microprobe (0.25 microns).

4.3 Clustering of Manganese

All figures which illustrate manganese segregation show that some

segregation occurs distant from free surfaces in small, randomly

distributed clusters of approximately equal size and shape. It is

possible that these clusters may be manganese sulfide inclusions.

Figure 42 is a photograph of sample 3B-2 and shows the sulfur distribution

as determined by the electron microprobe. Very little sulfur is present

and is definitely not associated with the regions of high manganese

content. Therefore, the clusters are not manganese sulfide inclusions.

Consideration of Figure 35 shows that the depth of the free surface

region affected by manganese segregation appears to be approximately

2.8 microns. Electro-sectioning results show this region to be

approximately one micron thick. It is probable therefore that the

clusters are less than 2.5 microns in diameter. .

Samples were observed with the optical metallograph (X2600). At

this magnification nothing was observed which might correspond to the

clusters observed with the electron microprobe.

Manganese clustering in this manner has been observed by others

and is not an uncommon effect.

4.4 Non-Equilbrium Segregation

Aust et al (13) attempt to explain excess grain boundary
hardening in terms of a coupled flow of vacancies and solute atoms to
vacancy sinks following a quench. A supersaturation of vacancies is
produced in a specimen following a high temperature anneal and a
quench to a lower temperature. The supersaturation is relieved by
annihilation at vacancy sinks. Sinks include grain boundaries, lattice
imperfections and free surfaces. If impurity atoms are associated with
a fraction of the vacancies, the flow of solute-vacancy complexes toward
vacancy sinks will cause an increase in solute concentration adjacent
to these sinks. The excess hardening in the region of the sinks is
believed to result from dissociation of vacancy-solute complexes and
formation of solute clusters producing asymmetrical defects. The
following discussion shows that this mechanism is unlikely to control
the segregation of manganese to free surfaces in iron at the manganese
concentrations employed in these experiments.

Consider an iron-manganese alloy and choose a volume of this
material having a cross-sectional area of one square centimeter extending
from the free surface to a depth of fifteen microns. Assume that the
excess manganese is found in a strip one micron below the free surface.
The volume of this region is $(1)(1)(1 \times 10^{-4}) = 1 \times 10^{-4} cm^3$. Assuming
this volume to be composed of iron it has a mass of $(7.86)(1 \times 10^{-4}) =$
7.86×10^{-4} gm. If 1% manganese is present, the mass of solute is
$(7.86 \times 10^{-4})(10^{-2}) = 7.86 \times 10^{-6}$ gm. In one particular case (specimen
1-5, Figure 32) the manganese content in this region was
found to be increased by 200% (Chapter 4.5). This represents an increase
of $(7.86 \times 10^{-6})(2.0) = 1.6 \times 10^{-5}$ gm of manganese. This amount of

manganese equals $(1.6 \times 10^{-5})(6.02 \times 10^{23})/(54.94) = 1.75 \times 10^{17}$

atoms. If following a quench all of the retained vacancies are

associated with manganese atoms 1.75×10^{17} vacancies are required.

Assume the excess vacancies diffuse from the region between one and

fifteen microns below the surface. The volume of this region is

$(1)(1)(14 \times 10^{-4}) = 14 \times 10^{-4}$ cm^3. Therefore, the vacancy concentration

must be at least $(1.75 \times 10^{17})/(14 \times 10^{-4}) = 1.25 \times 10^{20}$ vacancies/cm^3.

The atomic concentration of iron is $(6.02 \times 10^{23})/(7.86)(55.85) =$

1.4×10^{21} atoms/cm^3. Therefore, the non-equilibrium mechanism of

solute segregation requires an unreasonably high vacancy concentration.

Furthermore, this calculation assumes 100% association between

manganese atoms and vacancies (unreasonably high) and a diffusion

distance during the quench of fourteen microns (unreasonably high).

Therefore, all the evidence indicates that the solute segregation

observed cannot be explained by the model proposed by Aust et al (13).

The concentrations over which Aust et al (13) worked were in the range

of parts/million rather than /%, as in this case.

4.5 Equilibrium Segregation

McLean (14) discusses equilibrium solute segregation to grain

boundaries and suggests that the maximum degree of solute segregation

is equivalent to a monatomic grain boundary layer. The following

discussion shows that the enrichment of manganese observed is equivalent

to much more than a monolayer.

Consider an iron-manganese alloy and choose a volume of this

material having a cross-sectional area of 1 cm^2 extending from the free

surface to a depth of fifteen microns. Assume that the excess manganese

is found in a strip extending two microns below the free surface and a

region denuded of manganese exists from two to fifteen microns below

the surface. The average manganese concentration is assumed to be 0.9%. The volume of material assumed to be denuded of solute is $(1)(1)(13 \times 10^{-4}) = 13 \times 10^{-4} cm^3$. This volume is assumed to be iron and weighs $(13 \times 10^{-4})(7.86) = 1.02 \times 10^{-2} gm$. The weight of manganese normally present in this region is $(1.02 \times 10^{-2})(0.009) = 9.18 \times 10^{-5}$ gm. Area A1 (Figure 33) is $(0.8)(13) = 10.4$ weight percent manganese-microns. Area A2 is approximated by two triangles and is $(.55)(6.5) = 3.58$ weight percent manganese microns. Assume the weight of iron in the specimen between two and fifteen microns below the surface is represented by area A1. If this is true, the weight of manganese removed from this region following segregation is $(9.18 \times 10^{-5})(3.58)/(10.4) = 3.16 \times 10^{-5}$ gm. The volume of the strip containing the excess manganese is $(1)(1)(2 \times 10^{-4}) = 2 \times 10^{-4} cm^3$. The weight of iron in this volume is $(2 \times 10^{-4})(7.86) = 1.572 \times 10^{-3}$ gm. The weight of manganese is therefore $(1.572 \times 10^{-3})(0.009) = 1.42 \times 10^{-5}$ gm. The weight of manganese present in this region following segregation is $(3.16 \times 10^{-5}) + (1.42 \times 10^{-5}) = 4.58 \times 10^{-5}$ gm. Therefore the weight percent of manganese in this region is $(4.58 \times 10^{-5})/(157.2 \times 10^{-5}) = 2.9\%$. Each manganese atom has a volume of approximately $(54.94)/(7.2)(6.02 \times 10^{23}) = 1.2 \times 10^{-23} cm^3$. The diameter of each atom is $[(1.2 \times 10^{-23})/(5.236 \times 10^{-1})]^{1/3} = 2.84 \times 10^{-8}$ cm. Along a 1 cm. path $(1)/(2.84 \times 10^{-8}) = 3.52 \times 10^7$ atoms could be placed side by side. Therefore, one such layer 1 cm^2 contains $(3.52 \times 10^7)^2 = 12.4 \times 10^{14}$ atoms. The weight of manganese present in the two micron strip along the free surface is 4.58×10^{-5} gm. This weight is equal to $(4.58 \times 10^{-5})(6.02 \times 10^{23})/(54.94) = 5.03 \times 10^{17}$ atoms. Therefore, if the surface were covered with a layer of pure manganese, the number of manganese layers one atom thick would be $(5.03 \times 10^{17})/(1.24 \times 10^{15}) = 405$.

Therefore, there is more segregation occuring to the surface region than can be explained by a monolayer of manganese.

4.6 Segregation as a Function of Annealing Temperature

Segregation of manganese to free surfaces is not evident following anneals at or below $950^{o}F$. Since the annealing time was twenty-four hours it is possible that segregation is not evident because insufficient time was allowed for manganese diffusion. The following discussion shows this may be the case.

The diffusion coefficient of manganese in iron at $950^{o}F$ is 9.4 x 10^{-12} cm^2/sec. (Smithells (15) and Diffusion Data (16)). The distance an average manganese atom travels at $950^{o}F$ in twenty-four hours is about ($X = (Dt)^{1/2}$) 9 microns. This distance is of the same order as the depth of the manganese denuded region following segregation. This suggests that the segregation of manganese to the free surface is diffusion controlled.

4.7 Nickel Segregation

At $700^{o}C$ the diffusion coefficient of nickel in iron is 27 x 10^{-12} cm^2/sec. (16). Following a twenty-four hour anneal at $1400^{o}F$ ($759^{o}C$) an average nickel atom diffuses at least $((27 \times 10^{-12})(9.64 \times 10^{4}))^{1/2}$ = 15.3 microns. Therefore, the lack of nickel segregation to free surfaces cannot be attributed to insufficient time at the annealing temperature.

4.8 Second Phase Formation

A calculation in Chapter 4.5 shows that the weight percent manganese in the surface region, two microns thick, following segregation is 2.9%. Hansen (17) suggests that in iron alloys containing more than 3.2% manganese, cooling results in transformation of gamma into two martensitic

products. The surface topography of sample 1-5 was studied with the Department of Entomology's Scanning Electron Microscope. The dark region of Figure 43 is Face A observed in Figure 16, while the light region is Face B. Figure 43 shows that the specimen's topography remains uniform up to the edge. Sample 1-5 was etched in nital (98% alcohol, 2% nitric acid) to reveal any martensite. None was observed. This suggests that there is no second phase formation. It is concluded that during the anneal the manganese concentration does not exceed 3.2% and the free surface region remains within the ferrite range.

4.9 Similarities With Non-Equilibrium Segregation

Non-equilibrium solute segregation and the observed segregation of manganese to free surfaces in iron have several characteristics in common.

First, in both cases segregation occured in some solvent-solute systems but not in others and there is a correlation with the activity and distribution coefficients. The solute with an activity coefficient greater than one and a distribution coefficient less than one, manganese segregated to the free surface. The solute with an activity coefficient less than one and a distribution coefficient greater than manganese, nickel, does not segregate to free surfaces. When segregation did occur a specific heat treatment was involved. The width of the region affected by an increase in solute is much greater than the width of a grain boundary.

There are however, characteristics which are not common in both cases. There is no interaction effect between manganese and nickel. Also, solute segregation is not affected by the cooling rate in the

iron-manganese system. Since diffusion controls the segregation of manganese the non-equilibrium model can not apply. The non-equilibrium model proposed by Aust et al (13) applies to solute concentrations in the parts/million range.

4.10 Similarities With Equilibrium Segregation

Neither equilibrium solute segregation or the observed segregation to free surfaces in iron are functions of the cooling rate from the annealing temperature and neither are functions of time at the annealing temperature except that sufficient time must be provided for solute diffusion to occur.

However, several differences exist. First, more manganese segregates to free surfaces than can be explained by a monolayer of manganese atoms. Secondly, segregation of manganese to grain boundaries was not observed.

The question remains, why is manganese segregating and what form does the segregation take?

4.11 Solute-Dislocation Interaction

The possibility exists that the manganese atoms in the free surface region are associated with dislocations. Chapter 4.5 shows that 4.58×10^{-5} gm. of manganese are found in a strip extending two microns below the surface. This weight of manganese is composed of 1.42×10^{-5} gm. present as a result of alloying and 3.16×10^{-5} gm. present as a result of segregation. Assume only the manganese atoms present as a result of segregation are associated with dislocations and assume that one-half of the atomic sites along a dislocation core are occupied by manganese atoms. Fiore et al (18) suggests that this concentration is unreasonably high. A weight of 3.16×10^{-5} gm. of manganese equals $(3.16 \times 10^{-5})(6.02 \times 10^{23})/(54.94) = 3.47 \times 10^{17}$ atoms. Since the solute concentration along the dislocation is 50%, 6.94×10^{17} atoms represent

the total number of dislocation sites required to accomodate 3.16×10^{-5} gm. of manganese. Assume these dislocation sites have the diameter of an iron atom (2.84×10^{-8} cm, Chapter 4.5). A path of 6.94×10^{17} iron atoms, single file, constitutes a length of $(2.84 \times 10^{-8})(6.94 \times 10^{17})$ = 1.97×10^{10} cm. The dislocation density in a volume of material 2×10^{-4} cm^3. (Chapter 4.5) is $(1.97 \times 10^{10})/(2 \times 10^{-4}) = 9.85 \times 10^{13}$ cm^{-2}. Hull (19) suggests a dislocation density of 5×10^{11} cm^{-2} for a heavily colled rolled metal. In this case only the manganese atoms segregated to the free surface region were assumed to be associated with dislocations, furthermore the depth of the high manganese region was chosen to be two microns and an unreasonably high solute concentration along the dislocation line was assumed. These assumptions therefore result in the calculation of a lower required dislocation density than may actually be the case. Nevertheless, the dislocation density was calculated in this way is much greater than that which would be reasonable. Therefore, the increase in manganese concentration in the free surface region is not believed to be the result of solute-dislocation interaction.

Summary

Nickel does not segregate to grain boundaries or surfaces. Manganese is observed to segregate to free surfaces but not to grain boundaries. The degree of this segregation is too high to be explained by equilibirum or non-equilibrium models. The segregation of manganese is diffusion controlled. It is not believed that solute-dislocation interactions are important. There is no obvious mechanism to account for the segregation of manganese to free surfaces.

5. Conclusions

1. In an iron-nickel alloy there is no segregation of solute to free surfaces following an anneal at $1400^{\circ}F$. The nickel is evenly distributed throughout the iron matrix.

2. In an iron-manganese alloy the solute definitely segregates to free surfaces following a high temperature anneal. The maximum manganese concentration occurs close to the surface.

3. These regions of high manganese concentration are discontinuous and are approximately one micron wide. The manganese concentration drops very rapidly with distance below the surface so that at a depth of five to ten microns a minimum solute content is reached. At depths greater than ten microns the manganese concentration increases to a constant value corresponding to the bulk composition. Thus a zone is depleted in manganese with the atoms segregating to the surface.

4. There is no correlation between the width of the high manganese region and the cooling rate following a high temperature anneal.

5. The segregation of manganese to free surfaces is not a function of annealing time.

6. The segregation of manganese to free surfaces in iron is diffusion controlled.

7. The high manganese region is not associated with a second phase, oxide product or sulfide inclusion.

8. Segregation of manganese to grain boundaries is not observed.

9. The degree of manganese segregation is too high for either the equilibrium or non-equilibrium segregation models to apply or to be the result of solute-dislocation interaction.

10. There is no interaction effect between manganese and nickel. The nickel solute behaves as if manganese is absent and the manganese behaves as if it were the only solute.

References

1. Westbrook, J.H., and Aust, K.T., <u>Acta Metallurgical</u>, 1963, Vol. 11, p. 1151.

2. Aust, K.T., Hanneman, R.E.,Niessen, P., and Westbrook, J.H., <u>Acta Metallurgica</u>, 1968, Vol. 16, p. 291.

3. Aust, K.T., and Westbrook, J.H., <u>Acta Metallurgica</u>, 1971, Vol. 19, p. 521.

4. Floreen, S., and Westbrook, J.H., <u>Acta Metallurgica</u>, 1969, Vol. 17, p. 1175.

5. Hanneman, R.E., and Anthony, T.R., <u>Acta Metallurgica</u>, 1969, Vol. 17, p. 1133.

6. Bercovici, S.d., Niessen, P., and Byerley, d.d., <u>Scripta Metallurgica</u>, 1969, Vol. 3, p. 663.

7. Hultgren, R., Orr, R.L., Anderson, P.D., and Kelley, K.K., <u>Selected Values of Thermodynamic Properties of Alloys</u>, John Wiley and Sons, New York, 1963, p. 638.

8. Low, J.R., Stein, D.F., Turkalo, A.M., and Laforce, R.P., <u>Transactions of the Metallurgical Society of the AIME</u>, 1968, Vol. 242, p. 14.

9. Hanneman, R.E., and Aust, K.T., <u>Scripta Metallurgica</u>, 1968, Vol. 2, p. 235.

10. Raymond, E.L., <u>Corrosion</u>, 1968, Vol. 24, p. 180.

11. Morrison, H.M., and Blackburn, D.A., <u>Journal of Scientific Instrumentation</u>, 1966, Vol. 43, p. 655.

12. Jacquet, P.A., <u>Metallurgical Reviews</u>, 1956, Vol. 1

13. Aust, K.T., and Westbrook, J.G., <u>Lattic Defects in Quenched Metals</u>, Academic Press, New York, 1965, p. 771.

14. McLean, D., <u>Grain Boundaries in Metals</u>, Claredon Press, Oxford, 1957.

15. Smithells, C.J., <u>Metals Reference Book</u>, Butterworths, Toronto, 1957.

16. <u>Diffusion Data</u>, Diffusion Information Center, Columbus, Ohio, 1967, Vol. 1, p. 21.

17. Hansen, M., <u>Constitution of Binary Alloys</u>, McGraw-Hill, New York, 1958.

18. Fiore, N.F., and Bauer, C.L., <u>Binding of Solute Atoms to Dislocations</u>, Progress in Materials Science, 1967, Vol. 13.

19. Hull, D., <u>Introduction to Dislocations</u>, Pergamon Press, Toronto, 1958.

20. <u>Metals Handbook</u>, American Society for Metals, 1948.

21. Hume-Rothey, W., and Raynor, G.U., <u>The Structure of Metals and Alloys</u>, The Institute of Metals, London, 1962.

Tables

Table 1

Correlation between various solvent-solute systems and grain boundary

hardening, atomic size difference and distribution coefficient, after

Aust et al (2), p. 297.

Solvent	Solute	Relative hardness* $H_B - H_G$	Atom size difference (%)†	Distribution coefficient
Zn	Al	+	+4.4	<1
	Au	−	+5.1	>1
	Cu	−	−6.6	>1
Sn	Pb	+	+10.8	<1
	Sb	−	+1.9	>1
Pb	In	+	−10.3	<1
	Sn	+	−9.7	<1
	Ag	+	−17.7	<1
	Au	+	−17.7	<1
	Ca	−−	+12.6	>1
	U	−	−21.2	‡

   * Hardness of grain boundary (H_B) − hardness of grain (H_G). A + value indicates $H_B > H_G$ and a − value indicates $H_B < H_G$.
   † Per cent difference of Goldschmidt atomic radius of solute with respect to that of the solvent. A + value indicates a solute atom which is larger than a solvent atom and a −− value is the reverse.
   ‡ Phase diagram not established.

Table 2

Correlation between various solvent solute systems and activity

coefficient and grain boundary hardening, after Aust et al (2), p. 299.

Solute	Solvent	T_1 (°K)	T_2 (°K)	k*	γ_2^{L}*	$\Delta F_2^{S \to L}$* (cal/mole)	γ_2^{S}*	γ_2^{S}	$H_B - H_G$
Al	Zn	693	933	0.21	3.57	+660	27	>1	+
Au	Zn	693	1336	1.4	$<1 \times 10^{-6}$	+1420	$<2 \times 10^{-6}$	<1	−
Cu	Zn	693	1356	1.6	0.023	+1530	0.044	<1	−
Pb	Sn	505	600	0.08	3.9	+180	56	>1	+
Sb	Sn	505	903	3.3	0.20	+2060	0.47	<1	−
In	Pb	600	429	0.85	1.4	−310	1.3	>1	+
Sn	Pb	600	505	0.7	3.6	−320	3.9	>1	+
Ag	Pb	600	1234	0.04	8.7	+1400	710	>1	+
Au	Pb	600	1336	0.015	0.26	+1600	67	>1	+
Ca	Pb	600	1123	1.01	$<1 \times 10^{-8}$	+900	$<2 \times 10^{-8}$	<1	−

   * Evaluated at T_1.

Table 3

Correlation between various solutes in lead and the distribution

coefficient, after Westbrook et al (1), p. 1153.

Solute	Solid solubility in lead[7] At.%	Distribution coefficient k in lead[10][11]
Au	~0.11 @ 215°C	0.015
Ag	~0.19 @ 304°C	
	~0.013 @ RT[8]	0.04
Sn	29 @ 183°C	0.57
	2.0 @ RT[9]	
In	30 @ 173°C	0.8*

Table 4

Effect of cooling rate on the solute concentration in the grain

boundary region, after Bercovice et al (6), p. 664.

Effect of Cooling Rate, After Holding at 380°C for 15 min.

Rate of Cooling Deg. C/sec.	Measured at % Solute in Grain Boundary Region	% Change Between Bulk and Boundary Solute Concentration
Water Quenched	0.116	45
3.6	0.142	77.5
0.05	0.140	75
0.01	0.141	76.5
Measured Bulk Concentration	0.080	

Table 5

Atom Sizes, distribution coefficients and activity coefficients of

solutes in zinc, after Hanneman et al (9), p. 236.

Solute	Metallic Radius Å	k	γ^s
Pb	1.70	$< 10^{-4}$	$> 10^5$
Sn	1.62	~0.008	~860
Cd	1.51	~0.2	~25
Cu	1.28	~1.6	0.044
Zn	1.34		

Table 6

Experimental program presented in tabulated form.

Series	Sample Number	% Manganese	% Nickel	Annealing Time (hrs.)	Annealing Temp.(^{O}F)	Cooling Condition
1	1-1	1.019	0	5	1400	H_2 Cool
	1-2			10		
	1-3			15		
	1-4			20		
	1-5*			24		
	1-6			30		
	1-7			35		
2	2-1*	1.019	0		1400	H_2 Cool
	2-2				1250	
	2-3				1100	
	2-4			24	950	
	2-5				800	
	2-6				650	
	2-7				500	
3A	3A-1	1.019	0	24	1400	H_2 Quench
	3A-2*					H_2 Cool
	3A-3					Furnace Cool
	3A-4					Step Cool
3B	3B-1	1.115	0	24	1400	Furnace Cool
	3B-2					H_2 Cool
	3B-3					Step Cool
4	4-1	1.019	1.0	24	1400	H_2 Cool
	4-2					Furnace Cool
5	5-1	0	1.09	24	1400	Furnace Cool
	5-2					H_2 Cool
	5-3					Step Cool

* Specimens 1-5, 2-1 and 3A-2 are identical and are the same sample
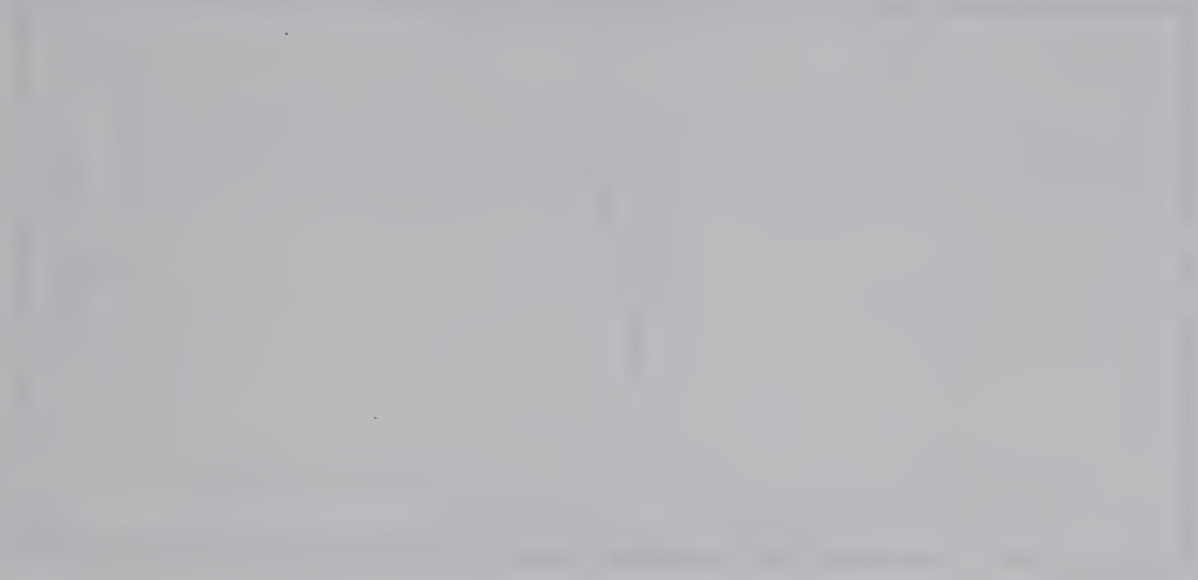
Figures
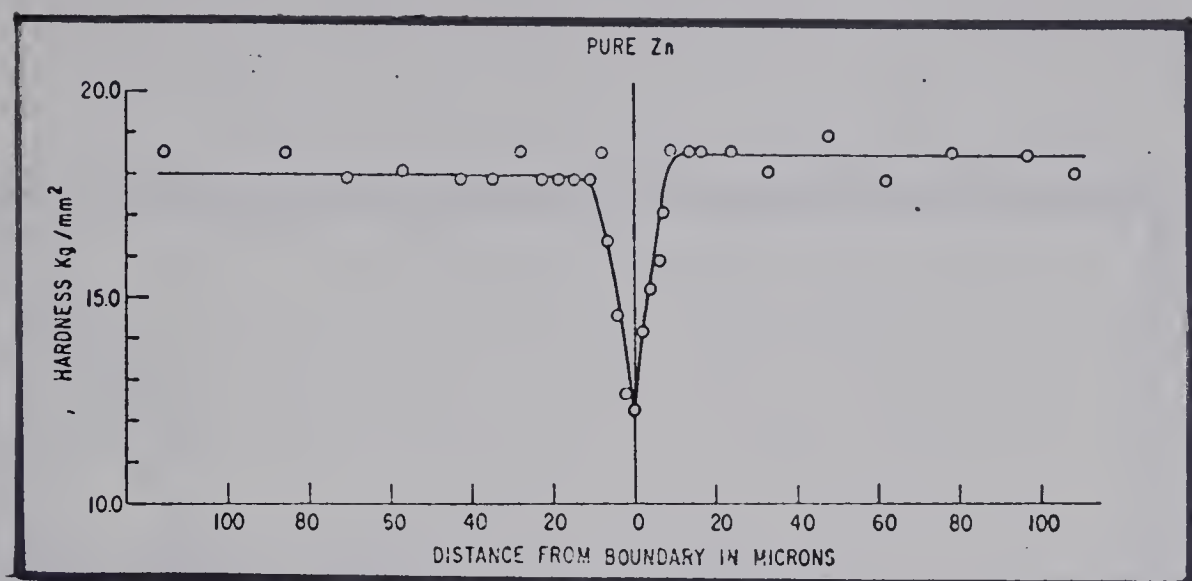
Figure 1

A hardness profile across a grain boundary in high purity zinc, after

Aust et al (2), p. 292.
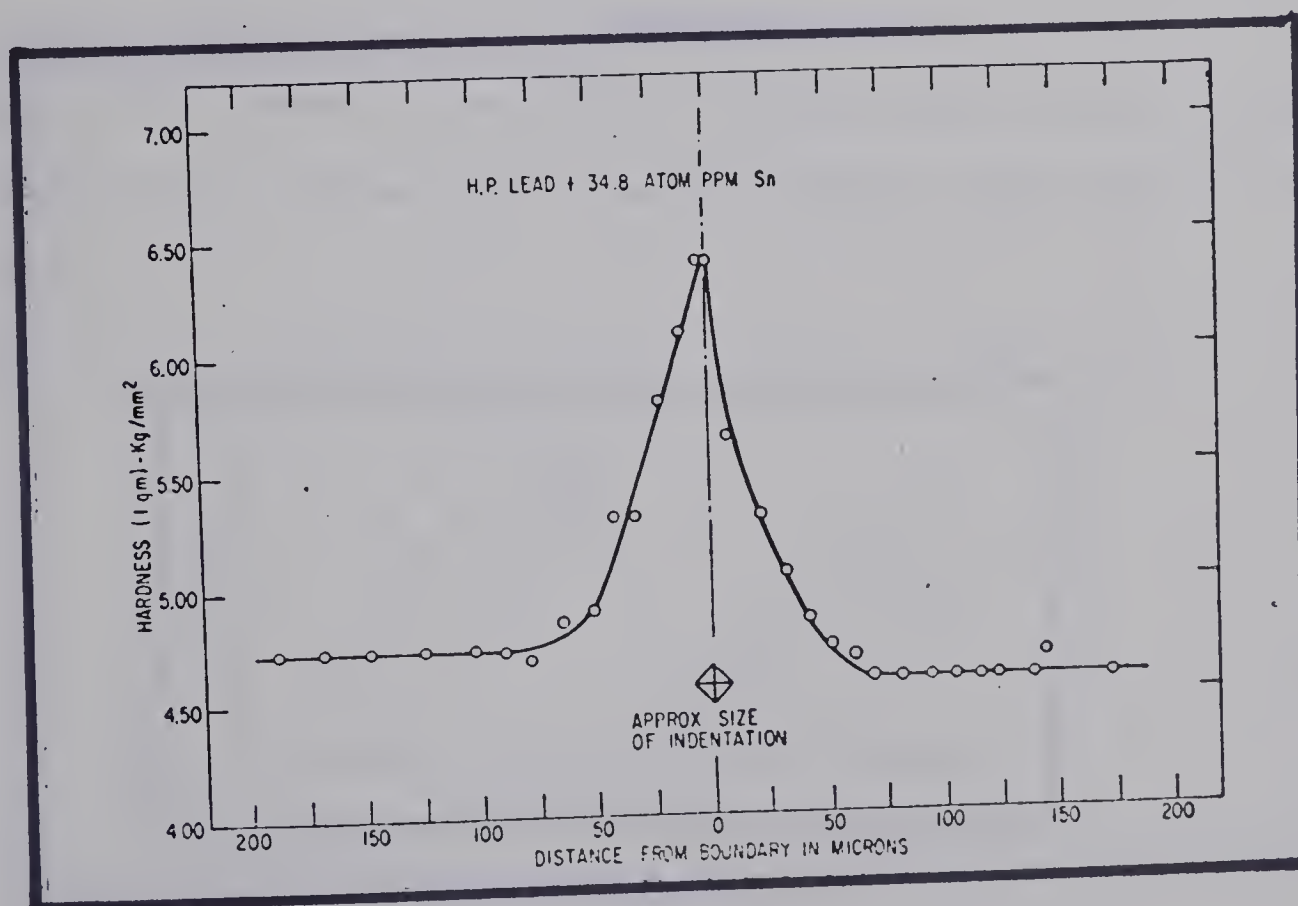
Figure 2

A hardness profile across a grain boundary in a lead-tin alloy, after

Westbrook et al (1), p. 1152.
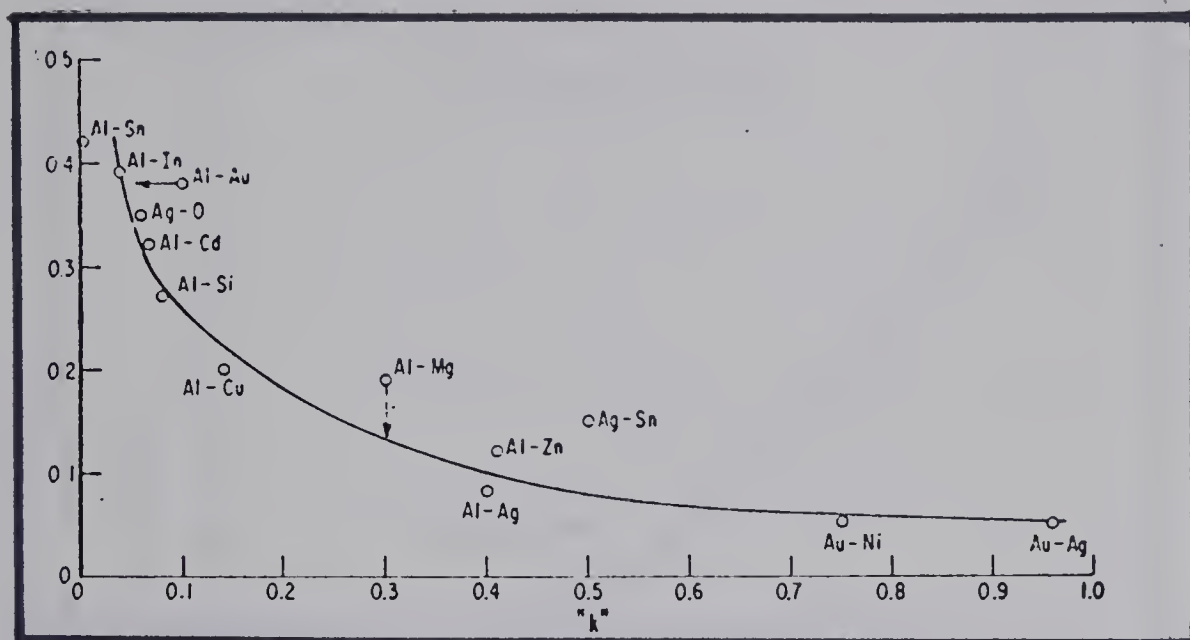
Figure 3

Relationship between vacancy-solute binding energy and distribution coefficient for various solvent-solute systems, after Aust et al (2), p. 298.
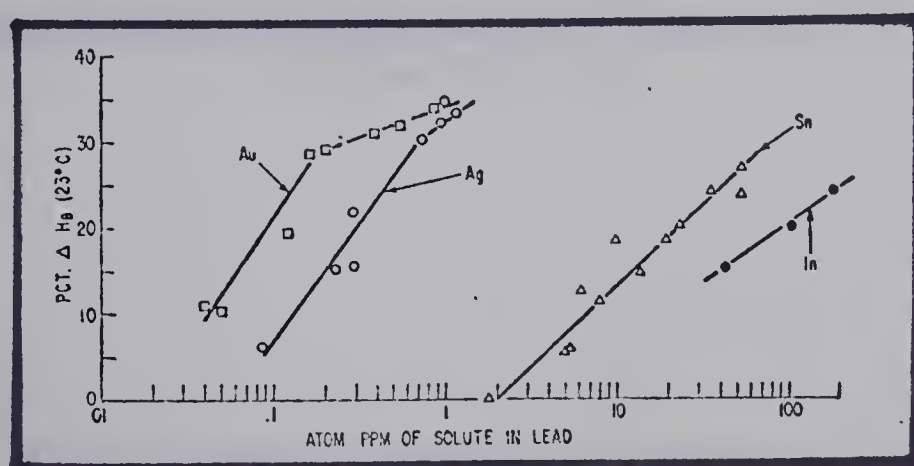
Figure 4

Concentration dependence of relative grain boundary hardening for gold, silver, tin and indium in lead, after Westbrook et al (1), p. 1152.
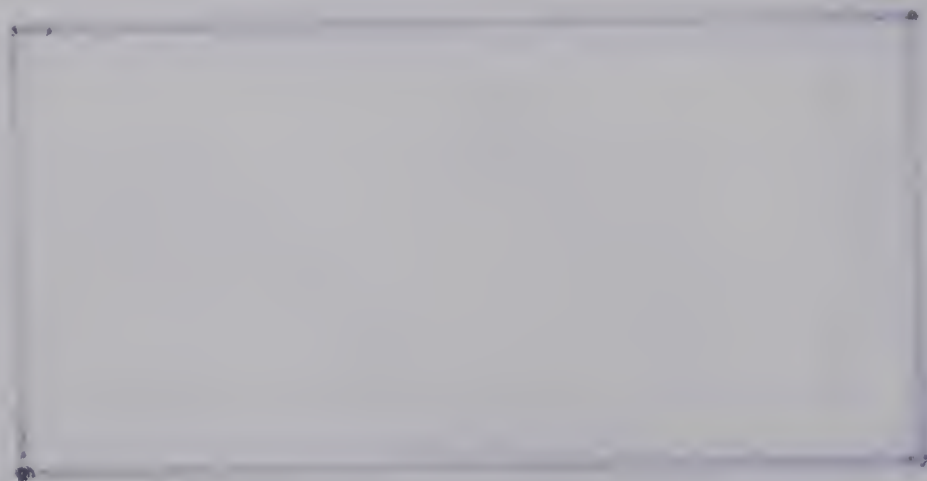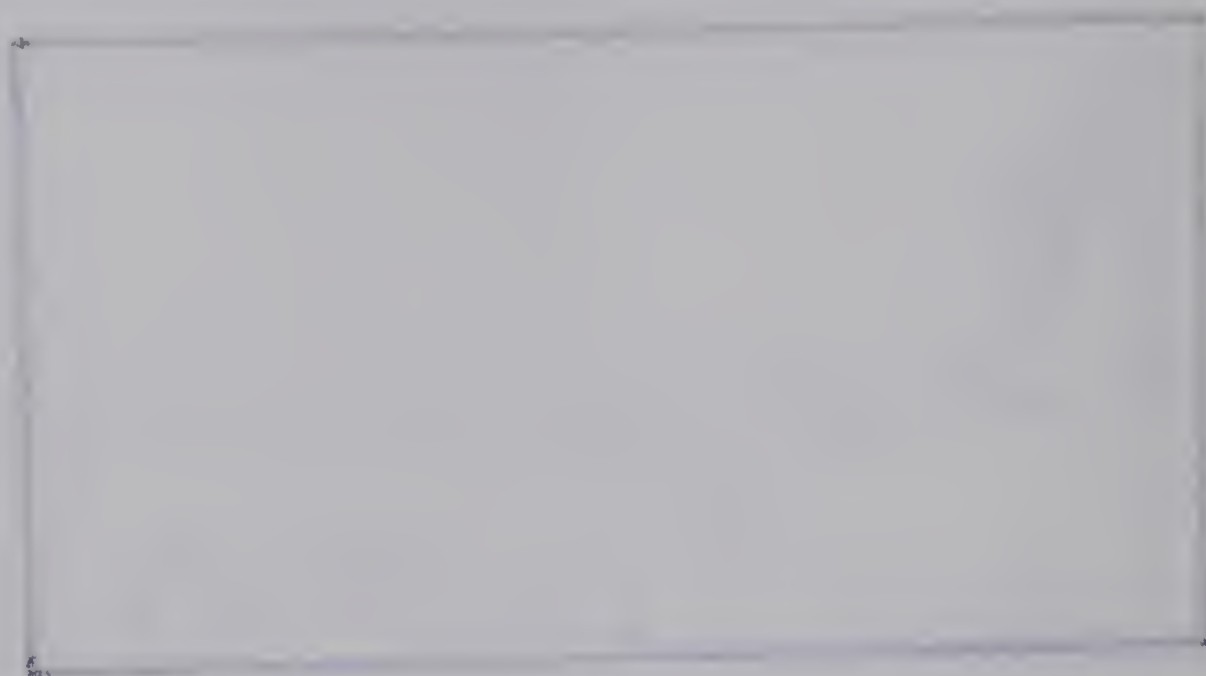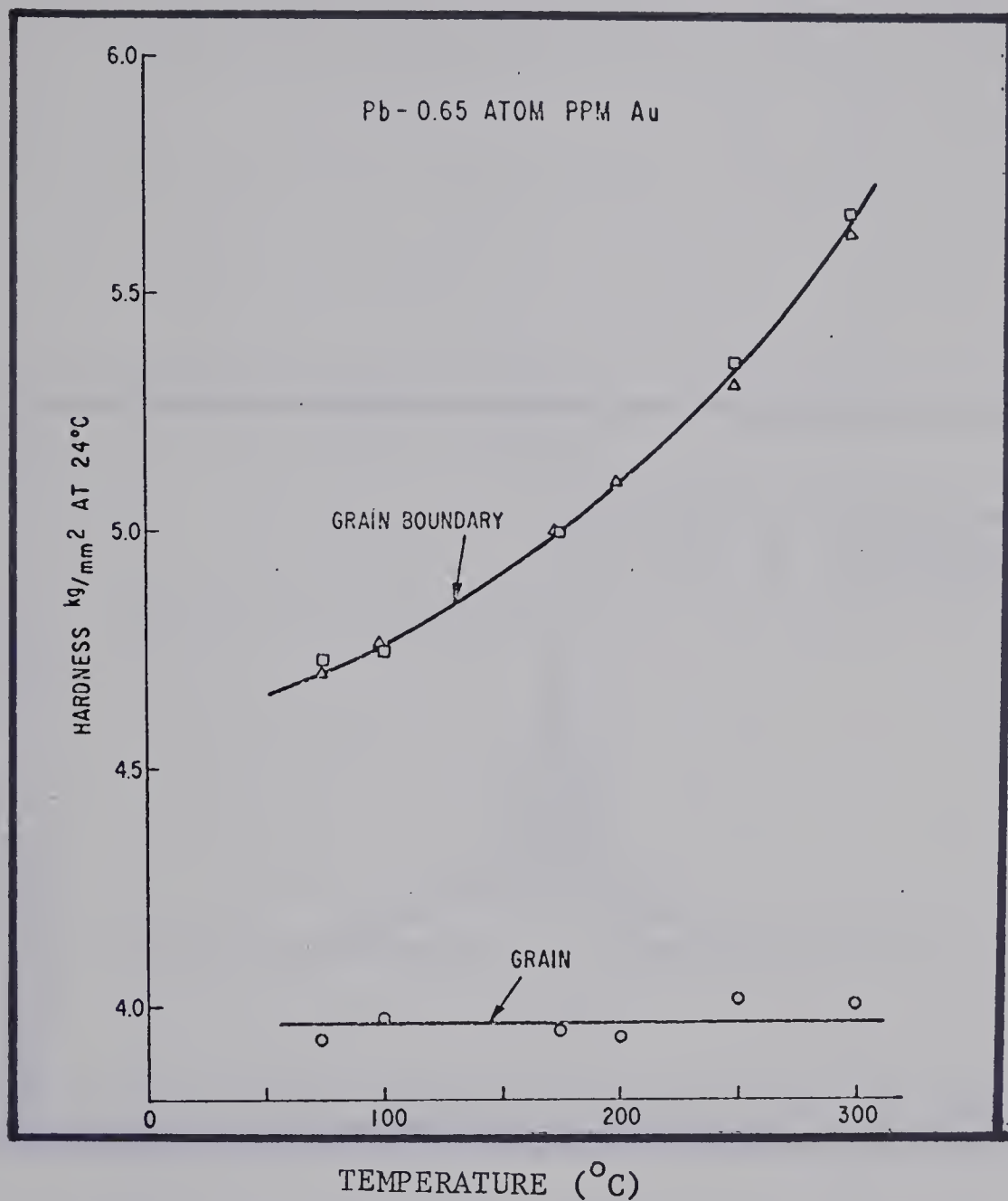
Figure 5

Influence of annealing temperature on the room temperature hardness of
a grain and a grain boundary, after Aust et al (13), p. 773.
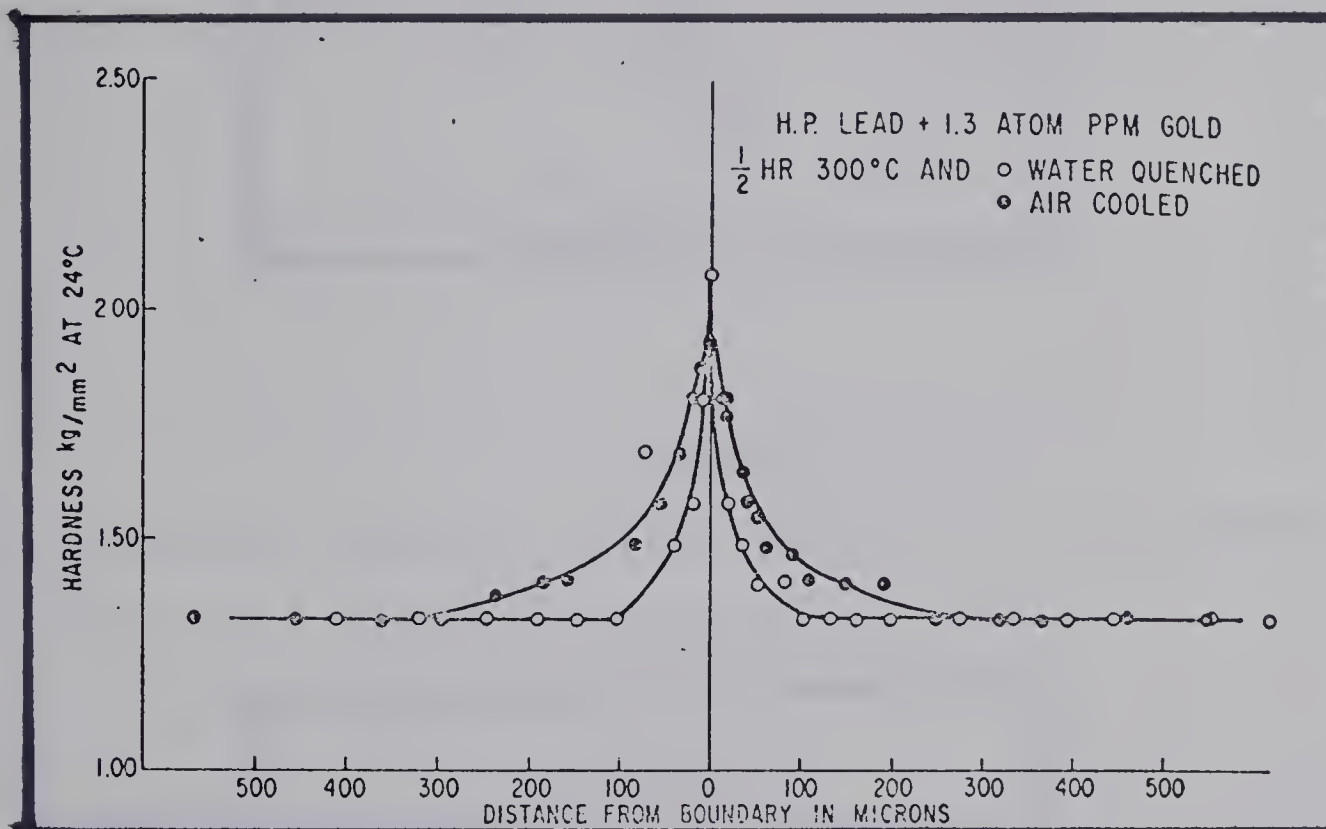
Figure 6

A hardness profile across a grain boundary in a lead-gold alloy following water quenching and air cooling from the annealing temperature (300°C), after Aust et al (13), p. 772.
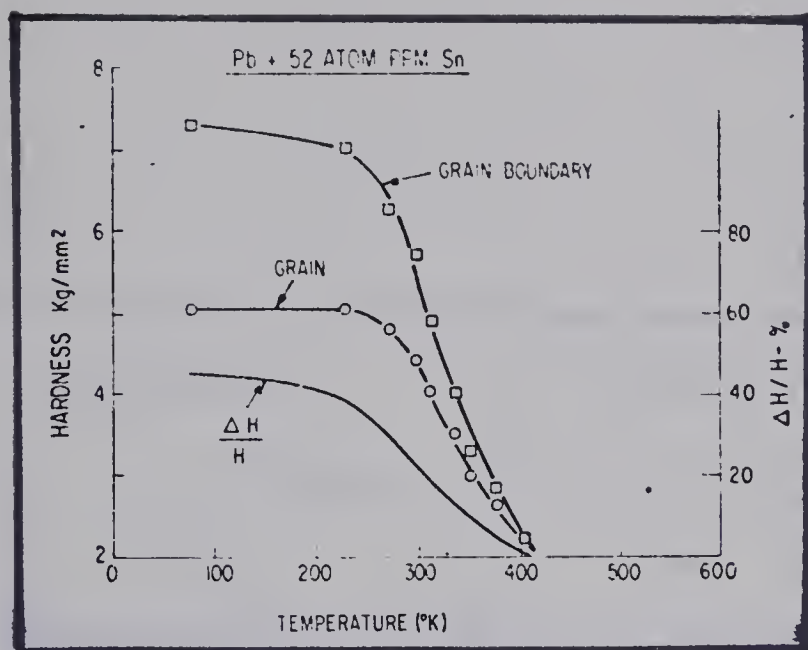
Figure 7

The temperature dependence of grain and grain boundary hardness in a lead-tin alloy, after Westbrook et al (1), p. 1154.
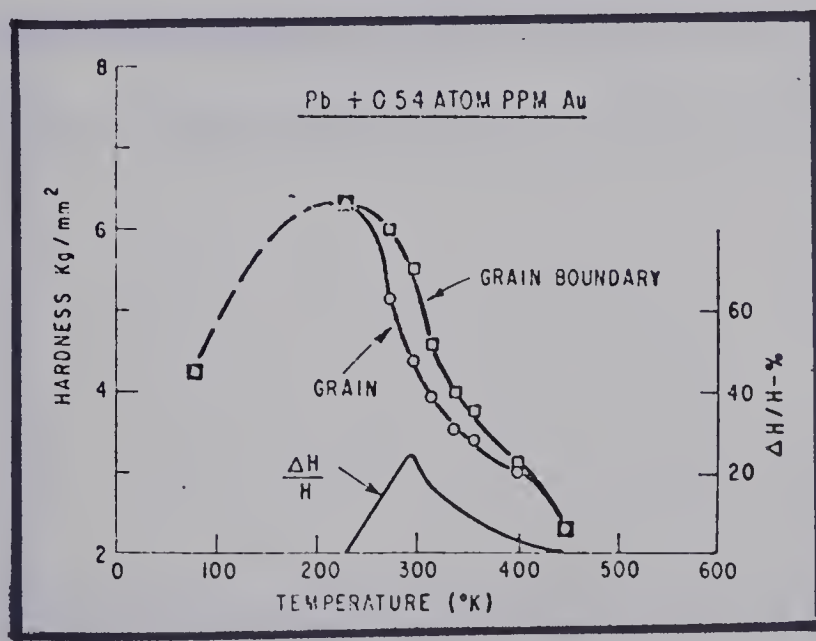
Figure 8

The temperature dependence of grain and grain boundary hardness in a lead-gold alloy, after Westbrook et al (1), p. 1154.
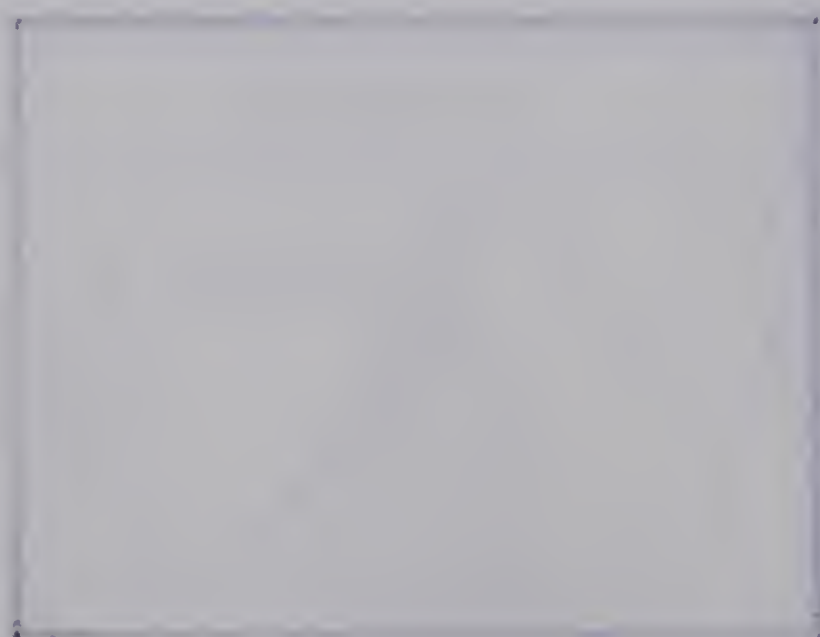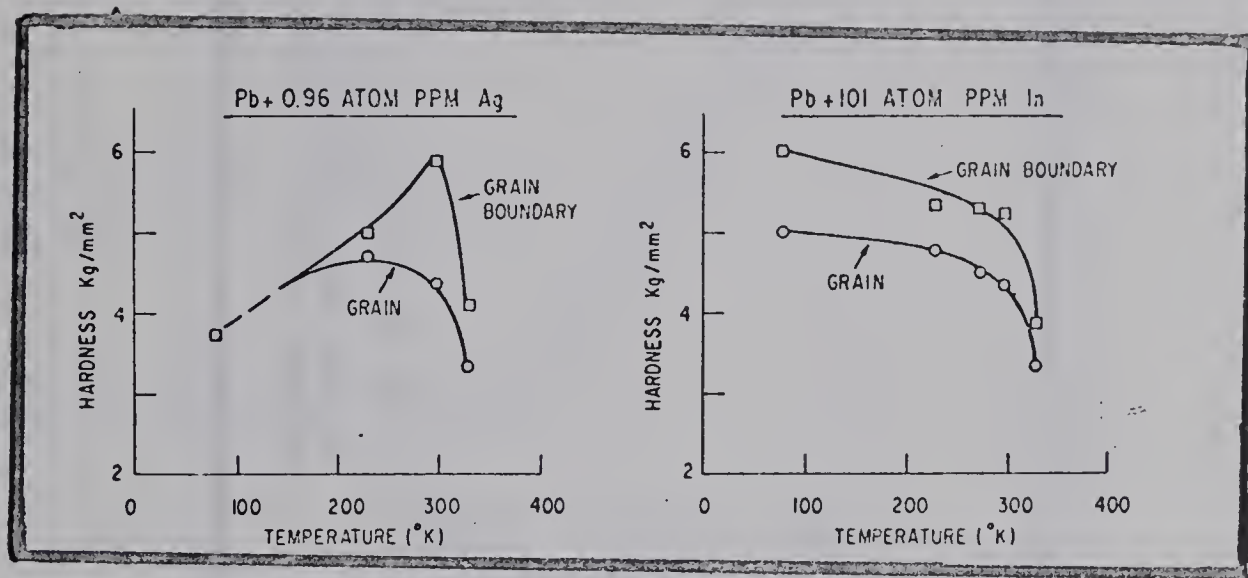
Figure 9

The temperature dependence of grain and grain boundary hardness in a lead-silver alloy, after Westbrook et al (1), p. 1154.
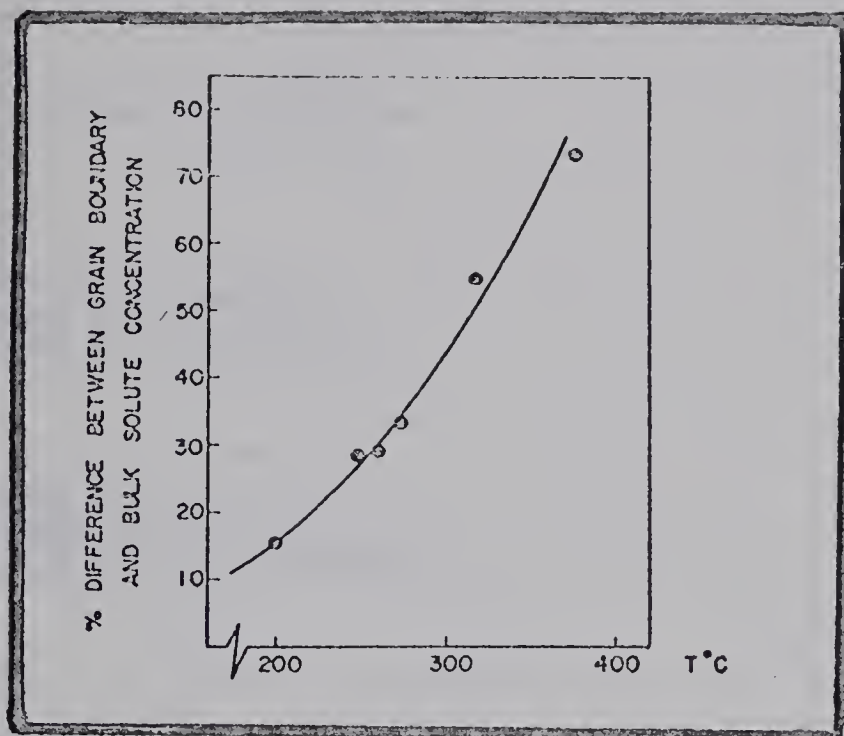
Figure 10

Percentage increase of solute concentration in the grain boundary region

with increasing annealing temperature, after Bercovici et al (6), p. 664.
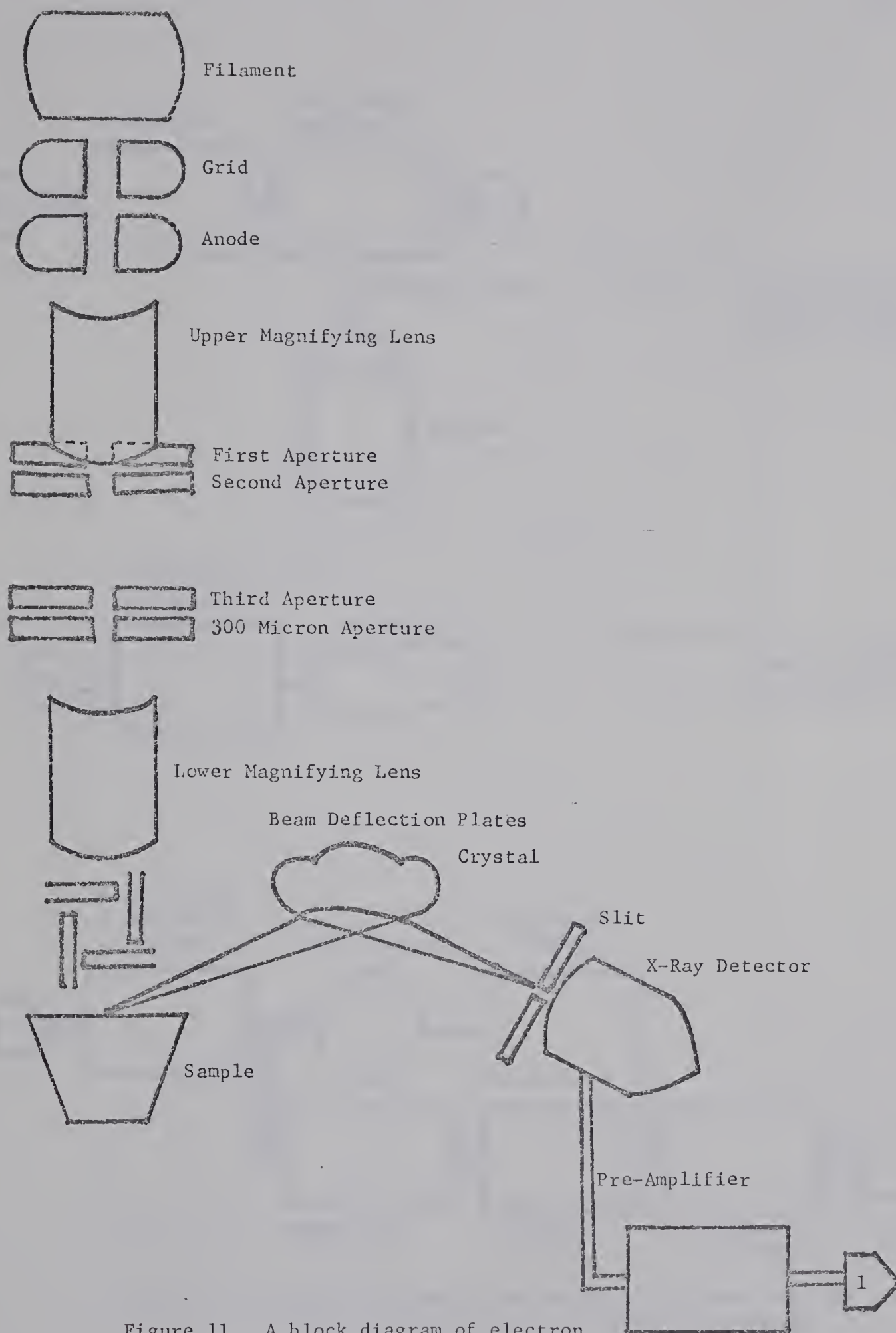
Figure 11. A block diagram of electron beam, x-ray and pre-amplifier systems of the electron microprobe.
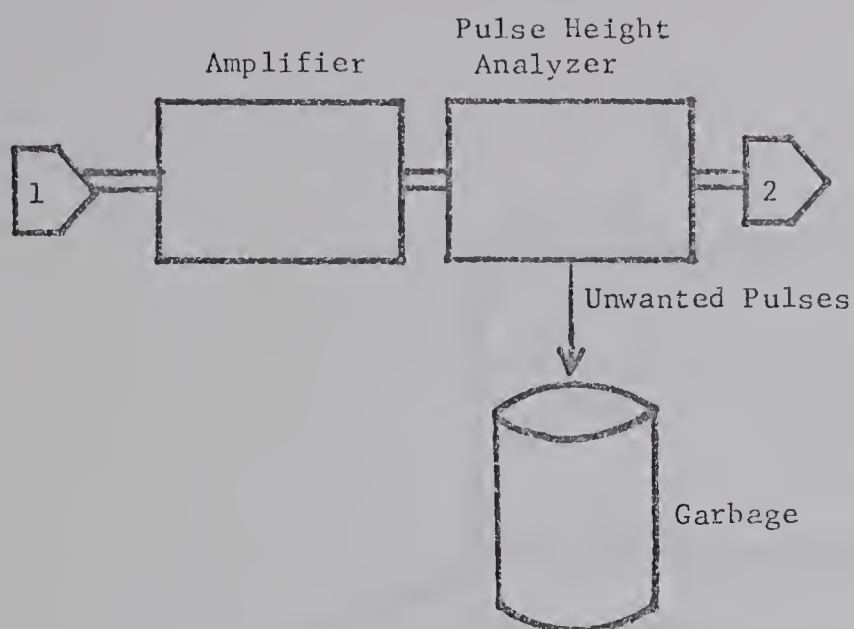
Figure 12. A block diagram of the amplifier and pulse height analyzer of the electron microprobe.
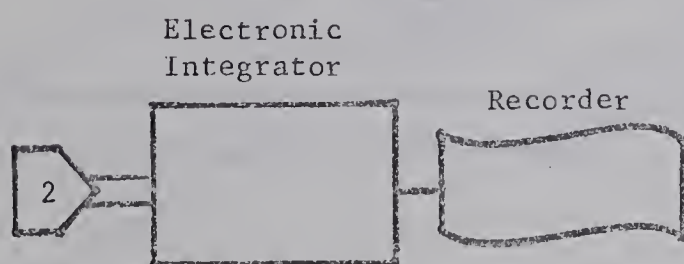
Figure 13. A block diagram of the x-y recorder of the electron microprobe.
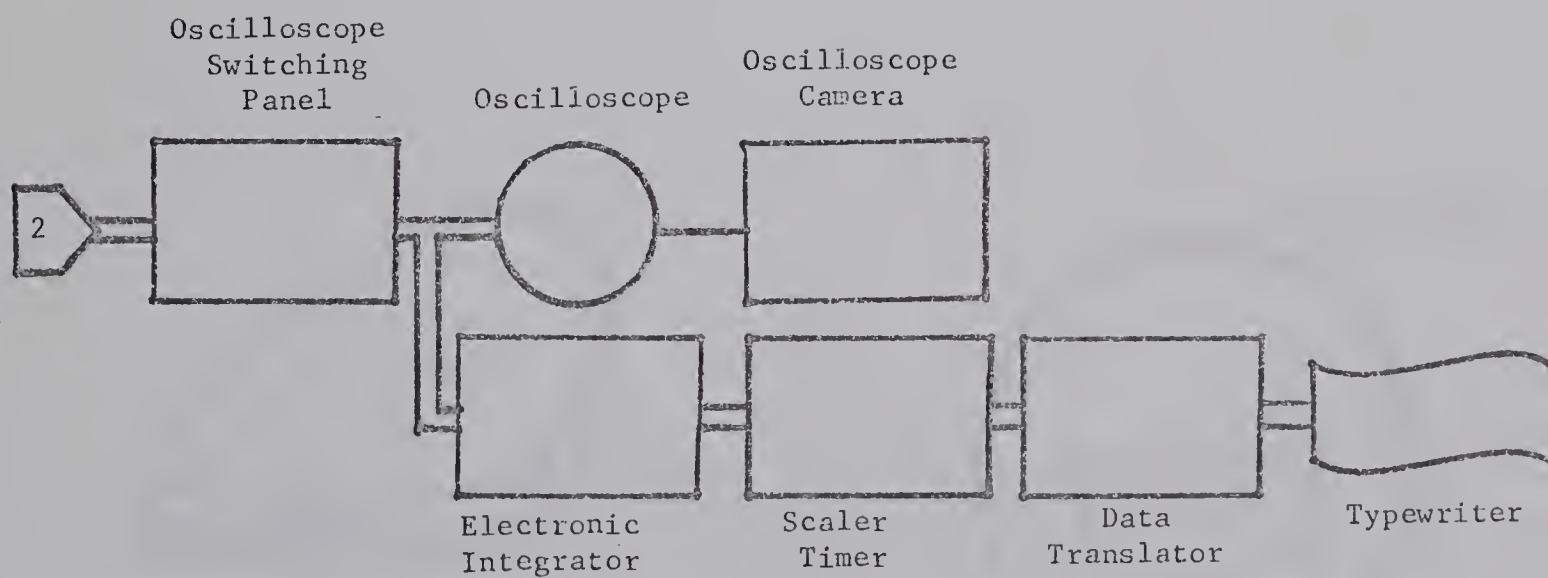
Figure 14. A block diagram of the oscilloscope camera and the typewriter printout of the electron microprobe.

Constant Voltage Source

1 ohm
resistor

Strip Chart
Recorder

Filter
Paper

Stainless
Steel
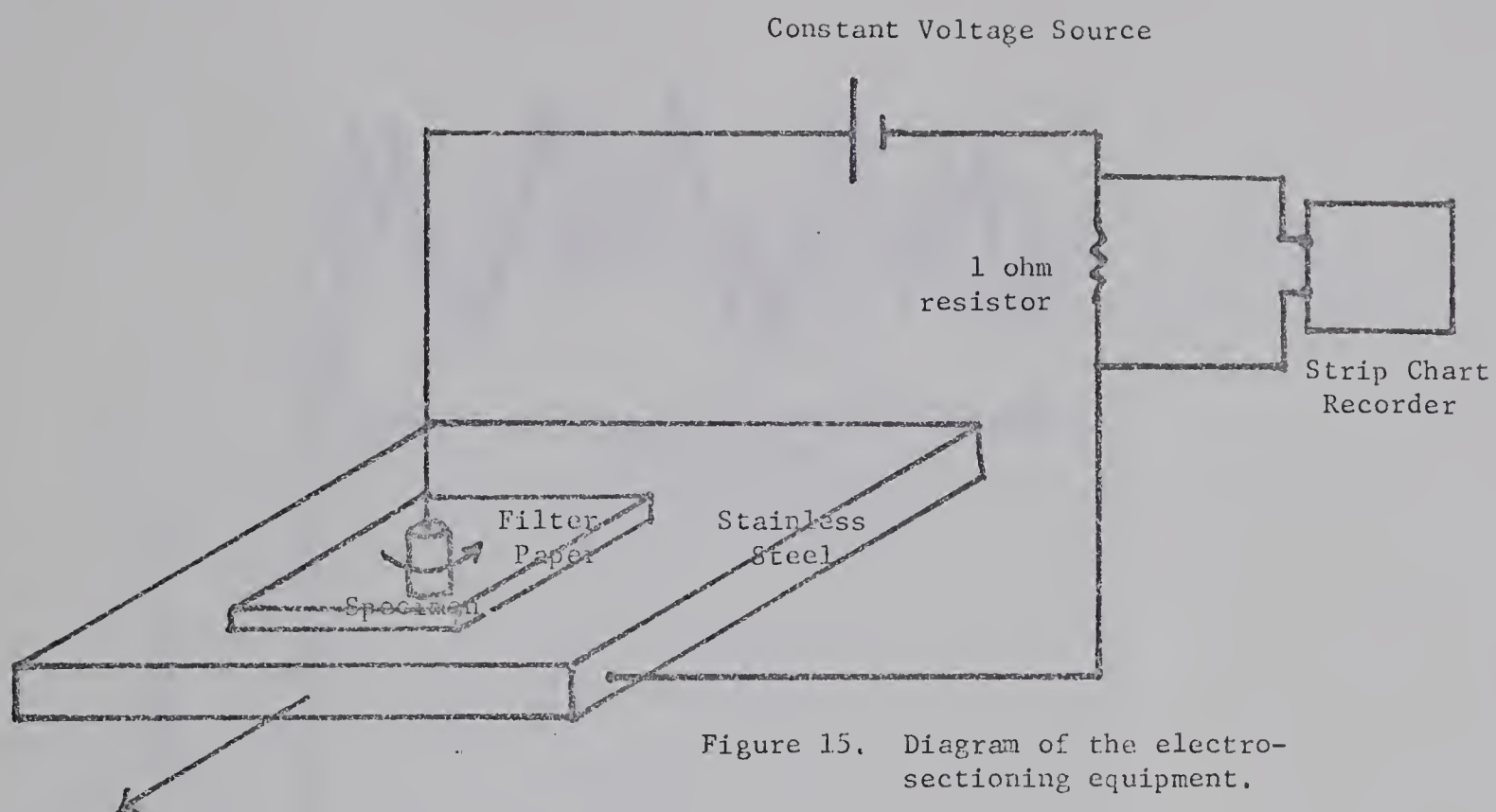
Specimen

Figure 15. Diagram of the electro-
sectioning equipment.

Face A

Face B

0.3 cm

0.9 cm
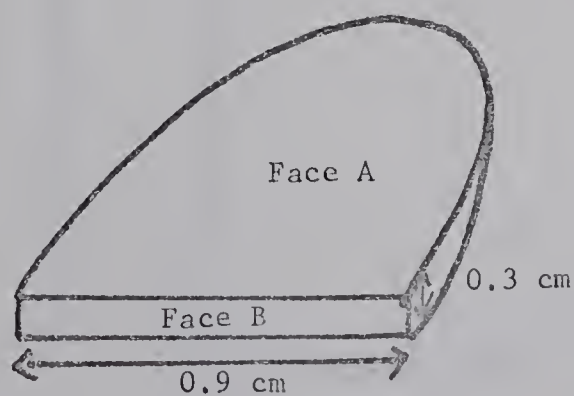
Figure 16. Diagram of an electron
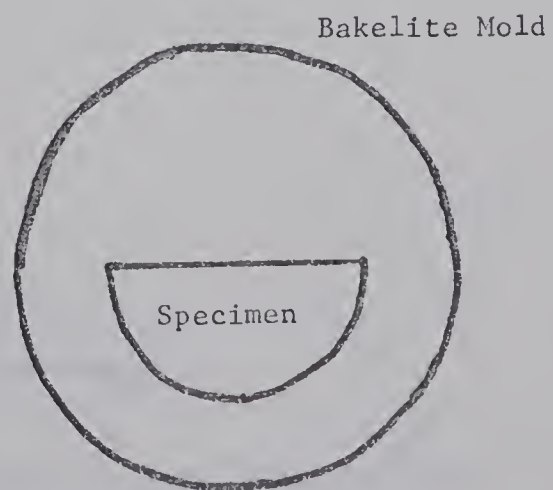microprobe specimen

Bakelite Mold

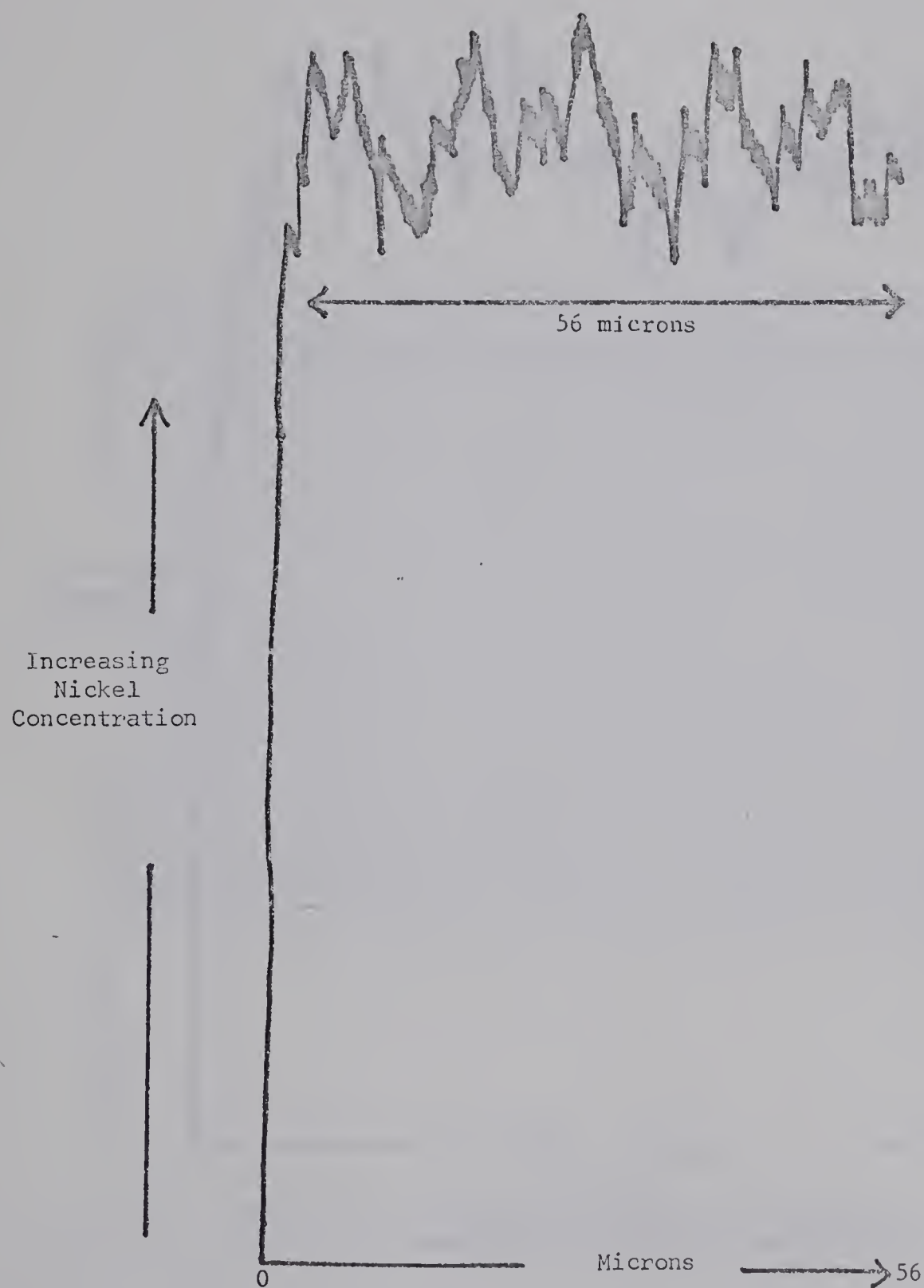Specimen

Figure 17. Diagram of an
electron microprobe
specimen in a
bakelite mold.

Figure 18. Variation in nickel concentration with depth below the free surface; specimen 5-1.
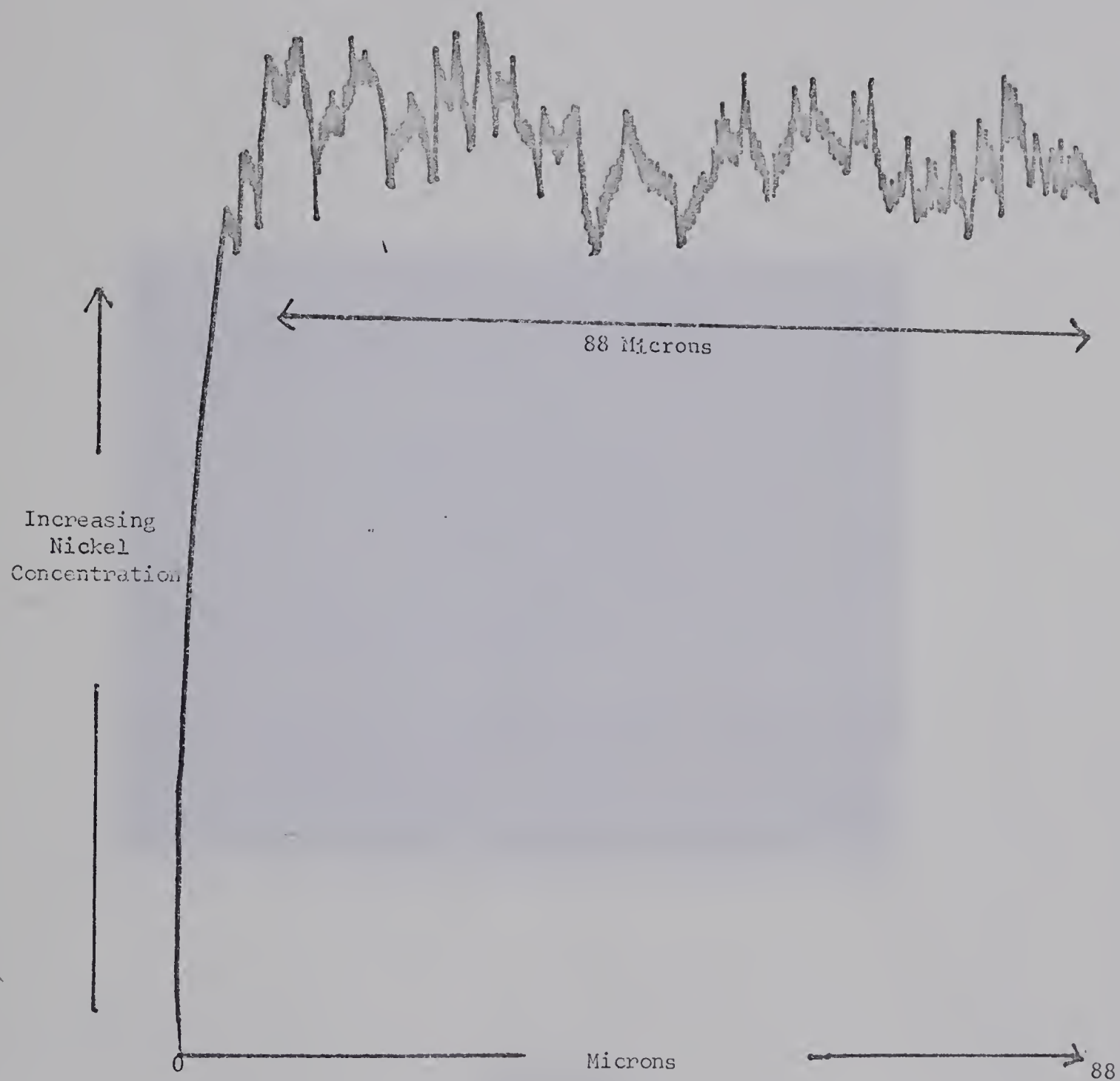
Figure 19. Variation in nickel concentration at a constant depth below the free surface, specimen 5-1.

Figure 20

Electron microprobe photograph of specimen 5-2 showing the nickel distribution resulting from an anneal at 1400°F. The long dimension of the photograph equals 600 microns.
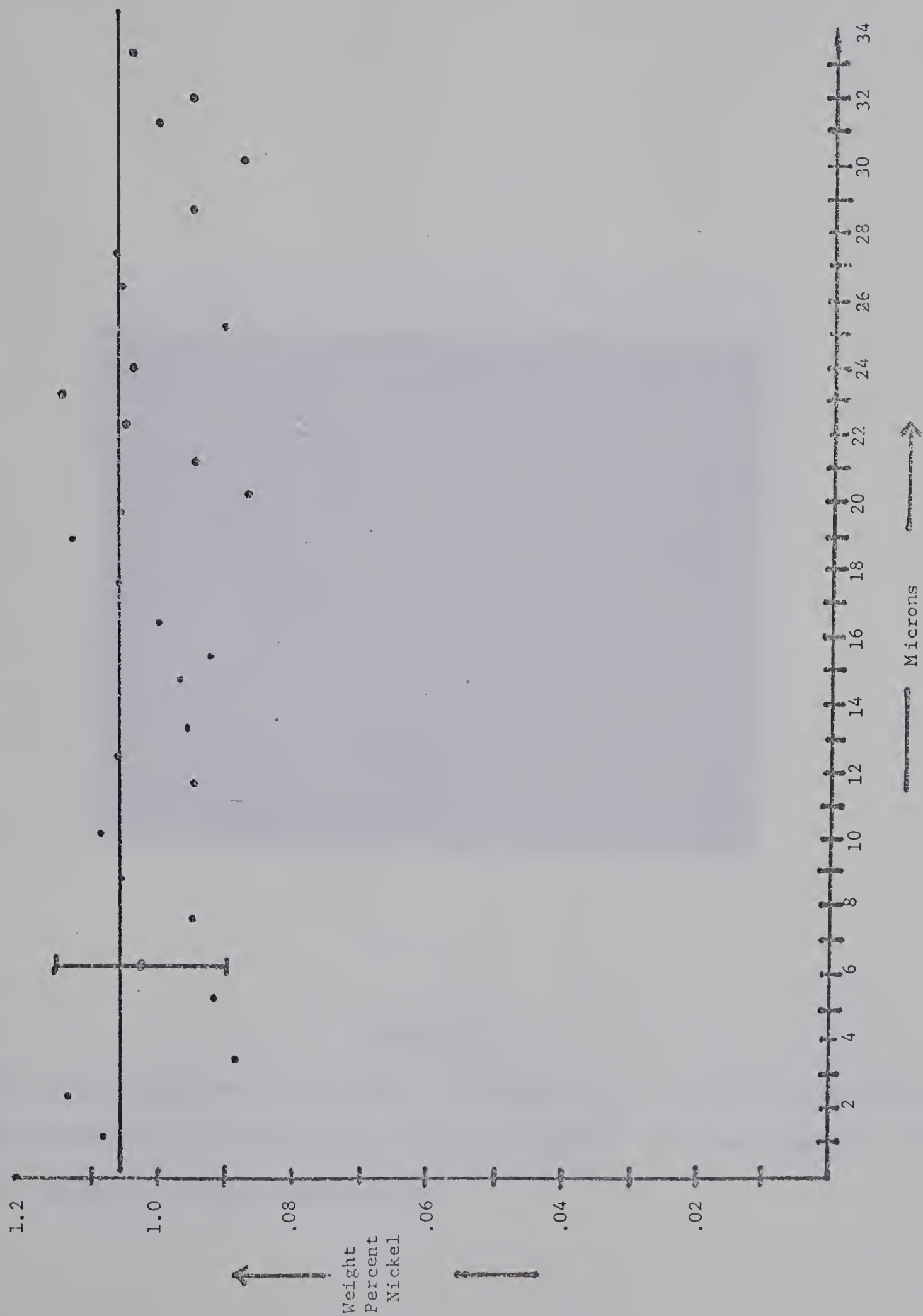
Figure 21. Variation in nickel concentration with depth below the free surface, determined by electro-sectioning, specimen 5-2.
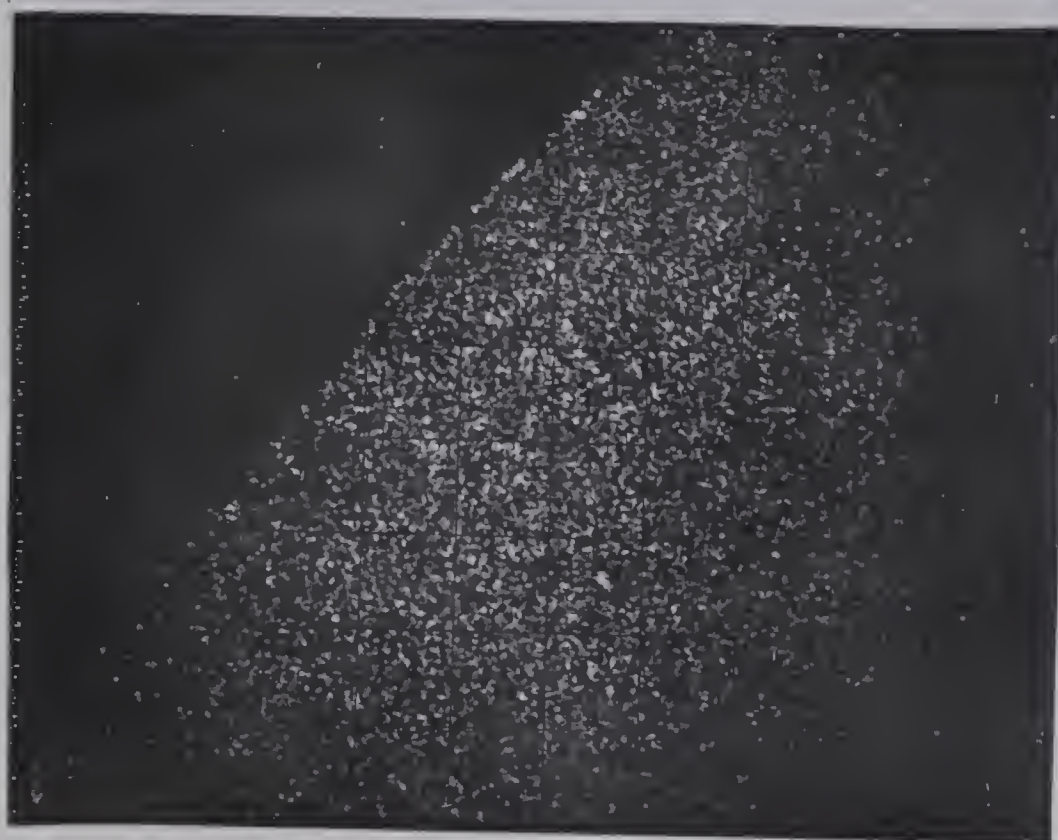
Figure 22

Electron microprobe of photograph of specimen 3B-1 showing the manganese distribution resulting from an anneal at 1400°F. The long dimension of the photograph equals 600 microns.

Figure 23

Electron microprobe photograph of specimen 3B-1 showing the manganese distribution resulting from an anneal at 1400°F. The long dimension of the phtotgraph equals 150 microns.

Figure 24

Electron microprobe photograph of specimen 3B-1 showing the manganese

distribution resulting from an anneal at 1400°F. The long dimension

of the photograph equals 38 microns.

Figure 25

Electron microprobe photograph of specimen 3B-2 showing the manganese

distribution resulting from an anneal at 1400°F. The long dimension
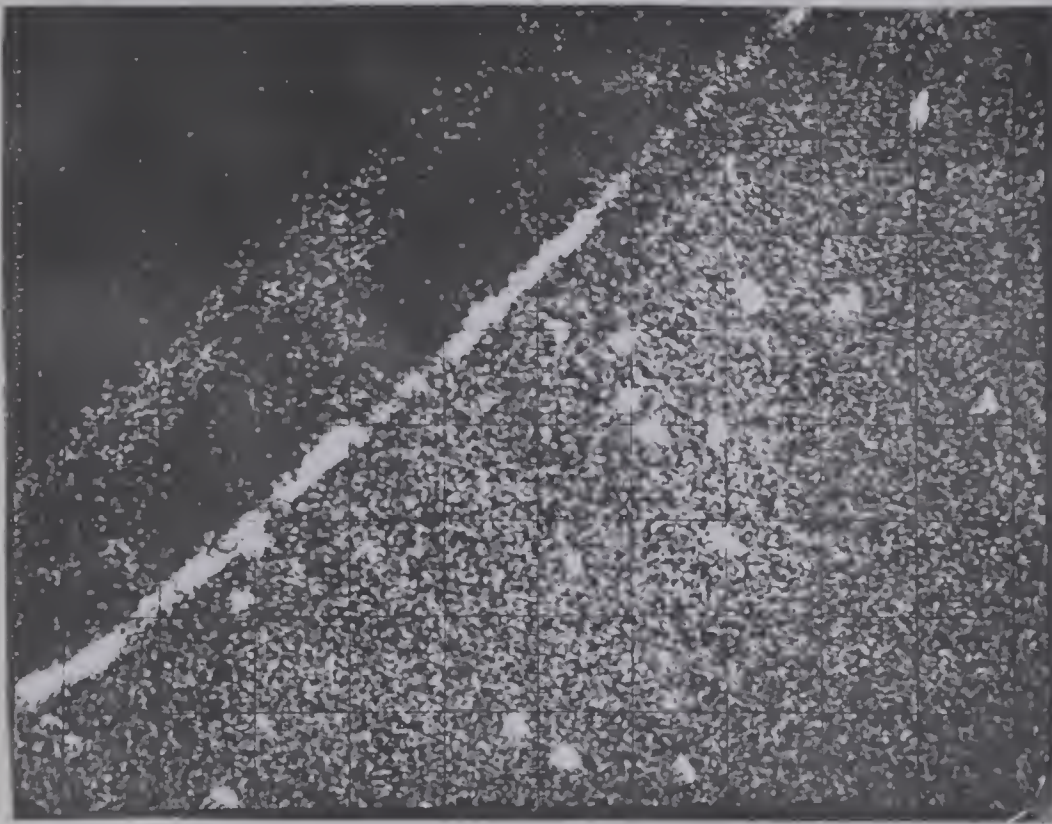
of the photograph equals 150 microns.

Figure 26

Electron microprobe photograph of specimen 3B-2 showing the manganese distribution resulting from an anneal at 1400°F. The long dimension of the photograph equals 150 microns.

Figure 27

Electron microprobe photograph of specimen 3B-3 showing the manganese

distribution resulting from an anneal at 1400°F. The long dimension

of the photograph equals 150 microns.

Figure 28

Electron microprobe photograph of specimen 3A-1 showing the manganese

distribution resulting from an anneal at 1400°F. The long dimension

of the photograph equals 75 microns.

Figure 29

Electron microprobe photograph of specimen 1-5, 2-1, 3A-2 showing the

manganese distribution resulting from an anneal at $1400^{O}F$. The long

dimension of the photograph equals 75 microns.
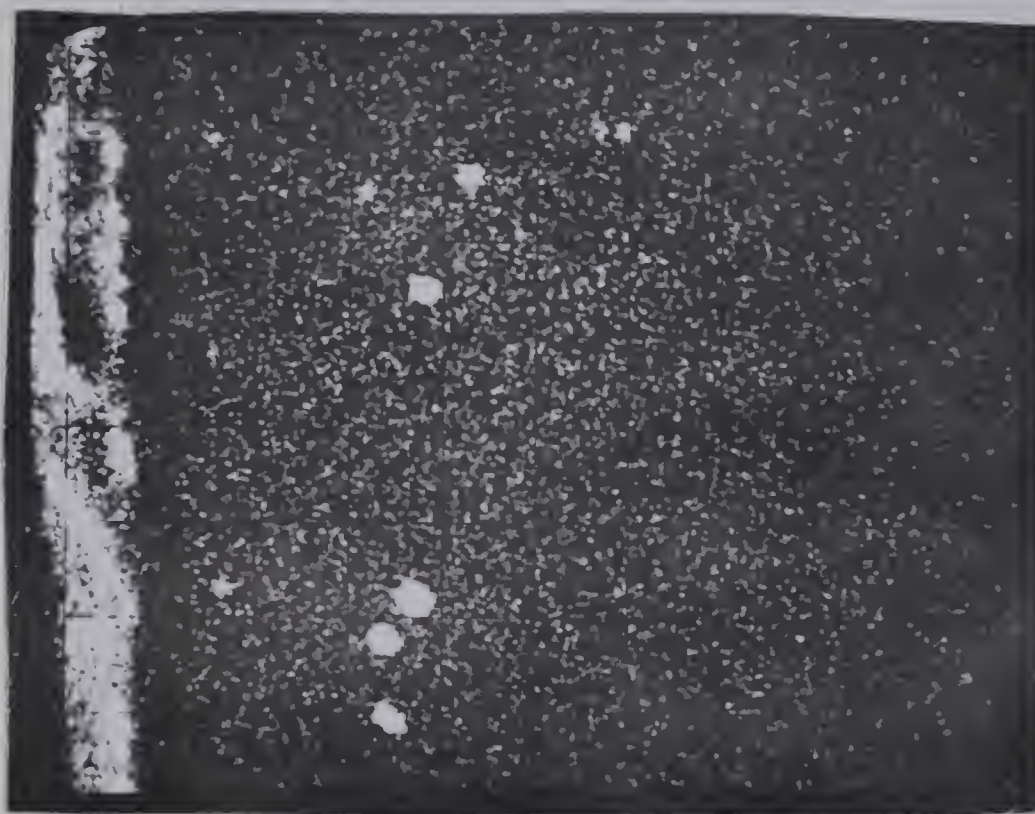
Figure 30

Electron microprobe photograph of specimen 3A-4 showing the manganese
distribution resulting from an anneal at 1400°F. The long dimension
of the photograph equals 75 microns.

Figure 30A. Variation in manganese concentration with depth below the free surface, determined with the electron microprobe, specimen 1-2.

Figure 31. Variation in manganese concentration with depth below the free surface, determined with the electron microprobe, specimen 1-5, 2-1, 3A-2.

Figure 32. Variation in manganese concentration with depth below the free surface, determined by electro-sectioning, specimen 1-5, 2-1, 3A-2.
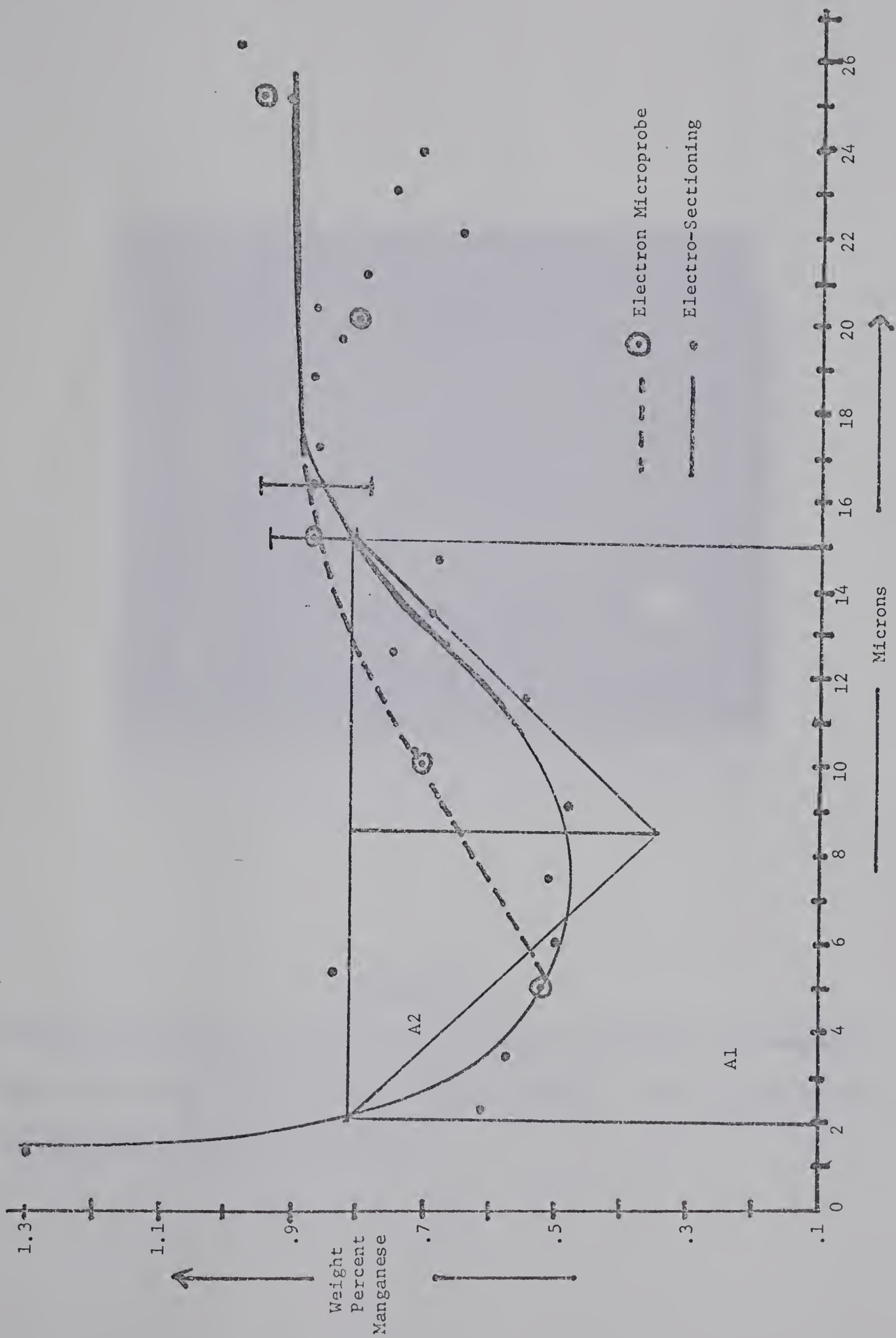
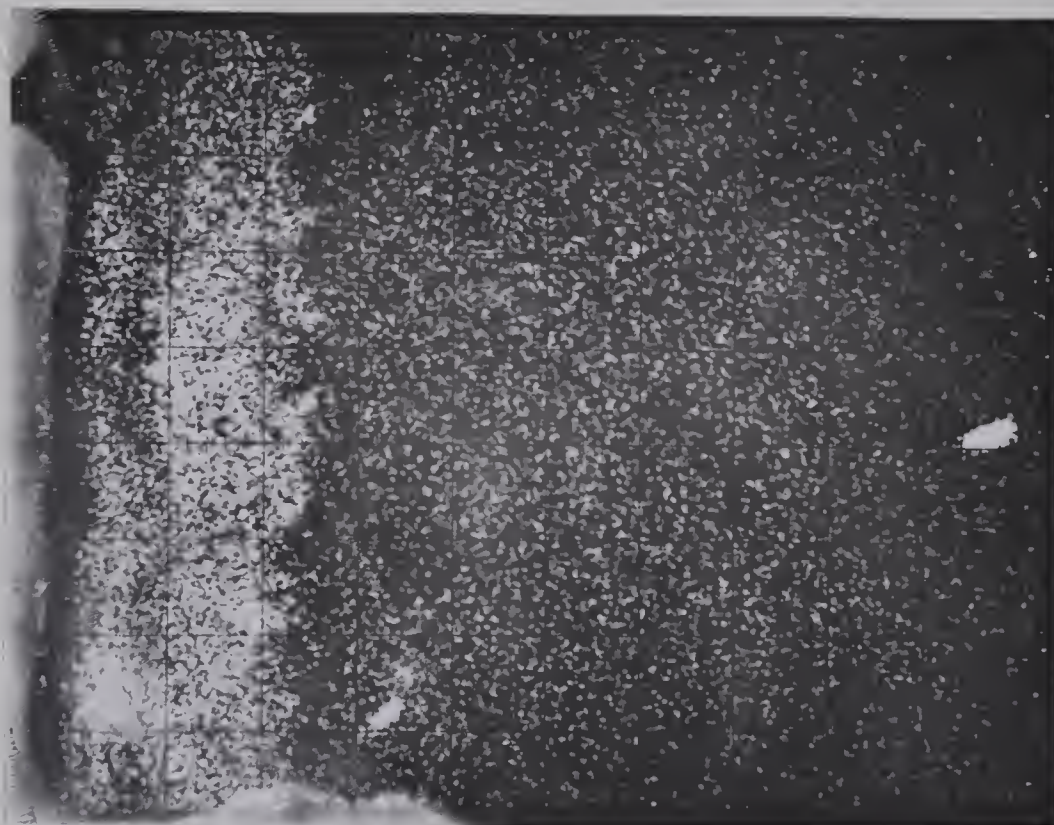Figure 33. Electron microprobe and electro-sectioning data of Figures 31 and 32 reproduced on one graph.

Figure 34

Electron microprobe photograph of specimen 1-7 showing the manganese distribution resulting from an anneal at $1400^{\circ}F$. The long dimension of the photograph equals 75 microns.
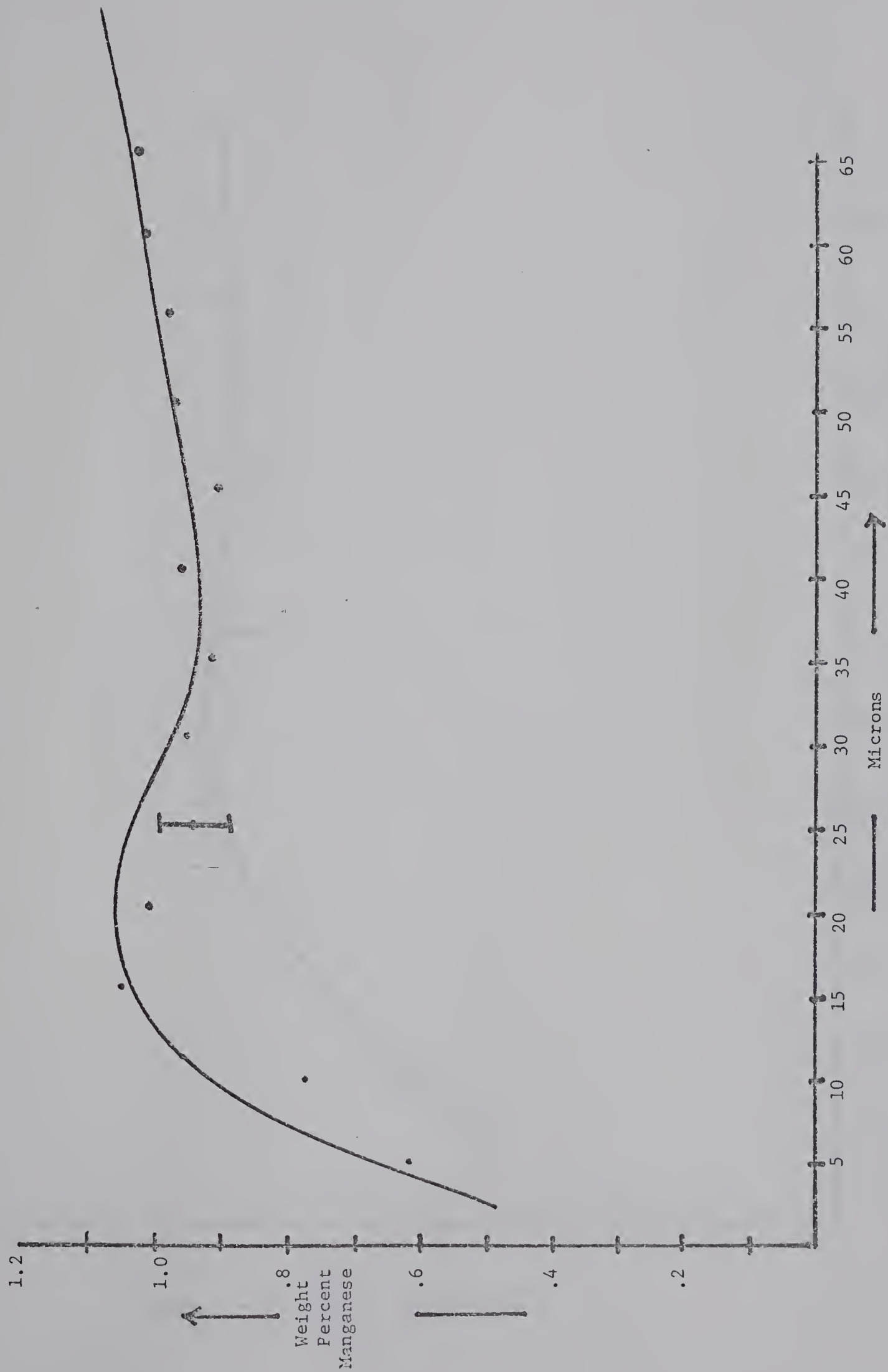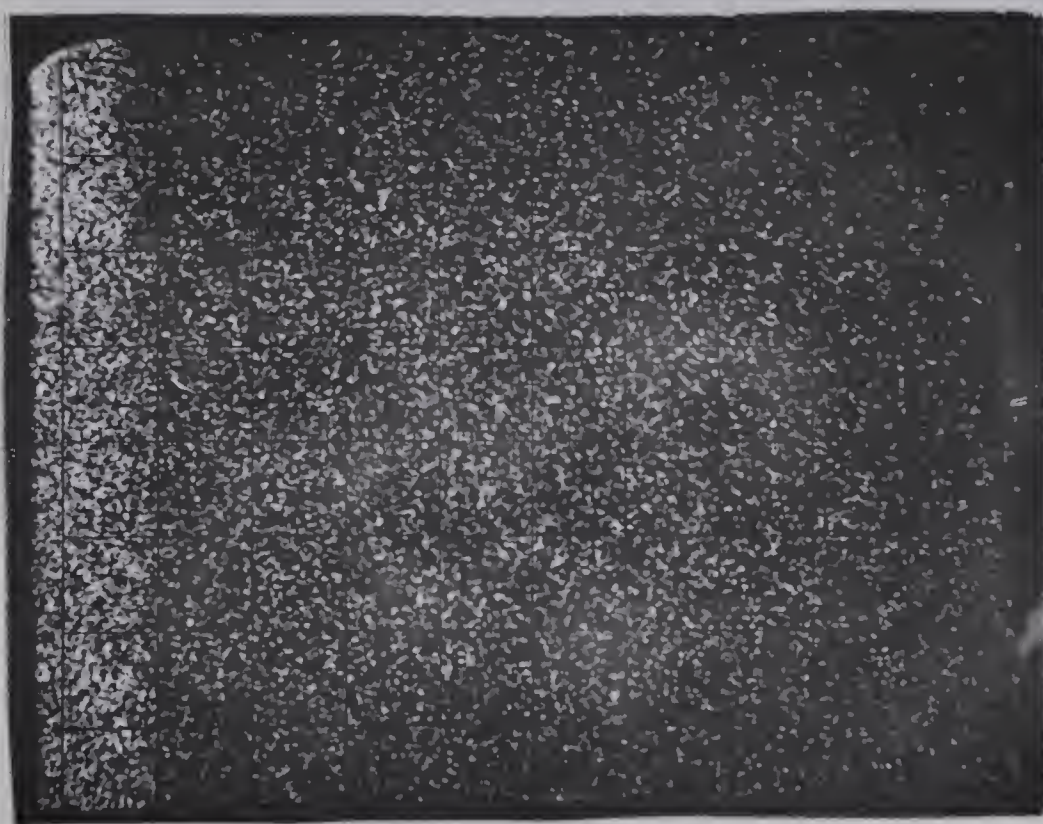
Figure 35

Electron microprobe photograph of specimen 2-3 showing the manganese distribution resulting from an anneal at 1100°F. The long dimension of the photograph equals 75 microns.

Figure 36

Electron microprobe photograph of specimen 2-7 showing the manganese
distribution resulting from an anneal at 500°F. The long dimension
of the photograph equals 75 microns.
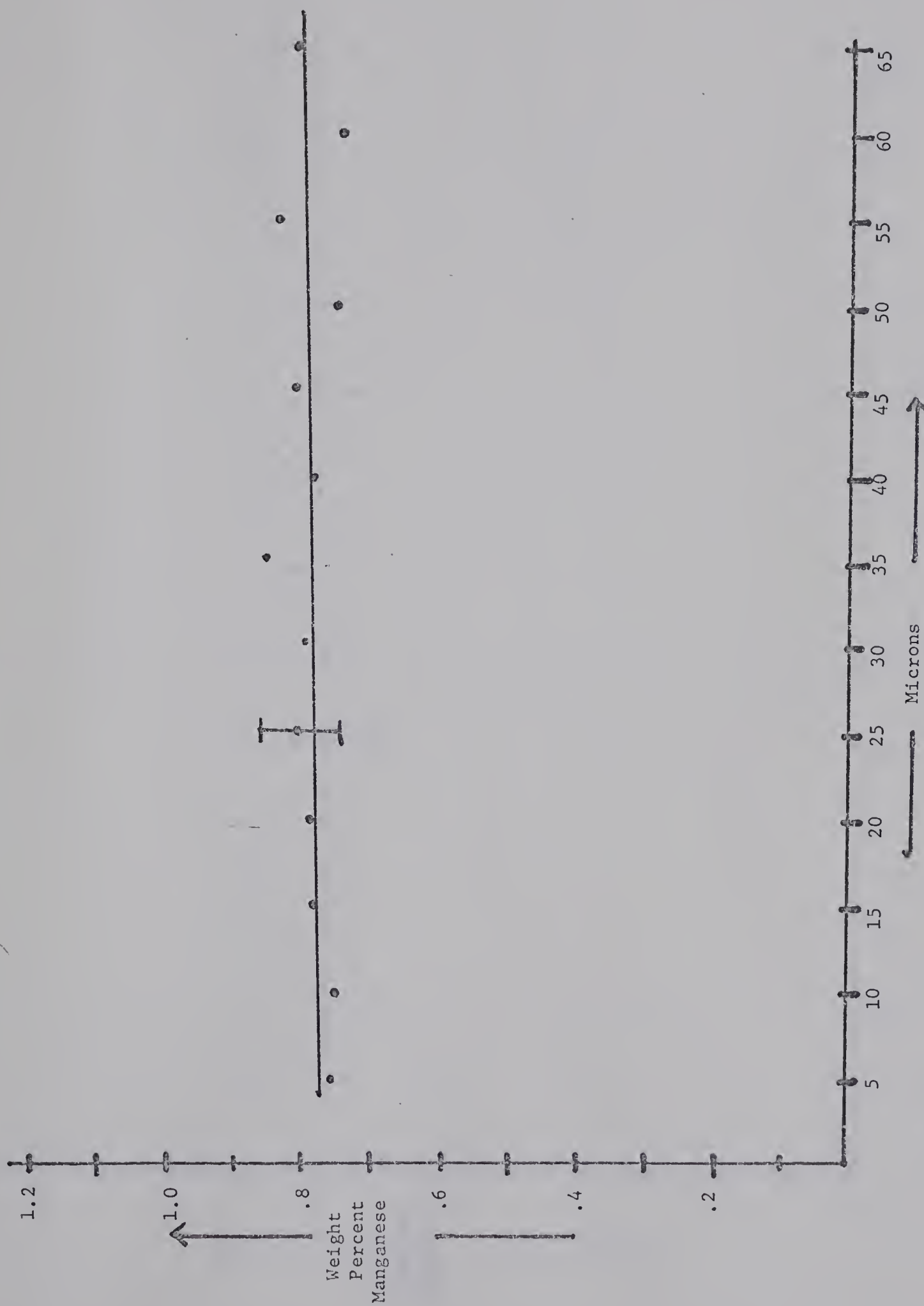
Figure 37. Variation in manganese concentration with depth below the free surface, determined with the electron microprobe, specimen 2-4.
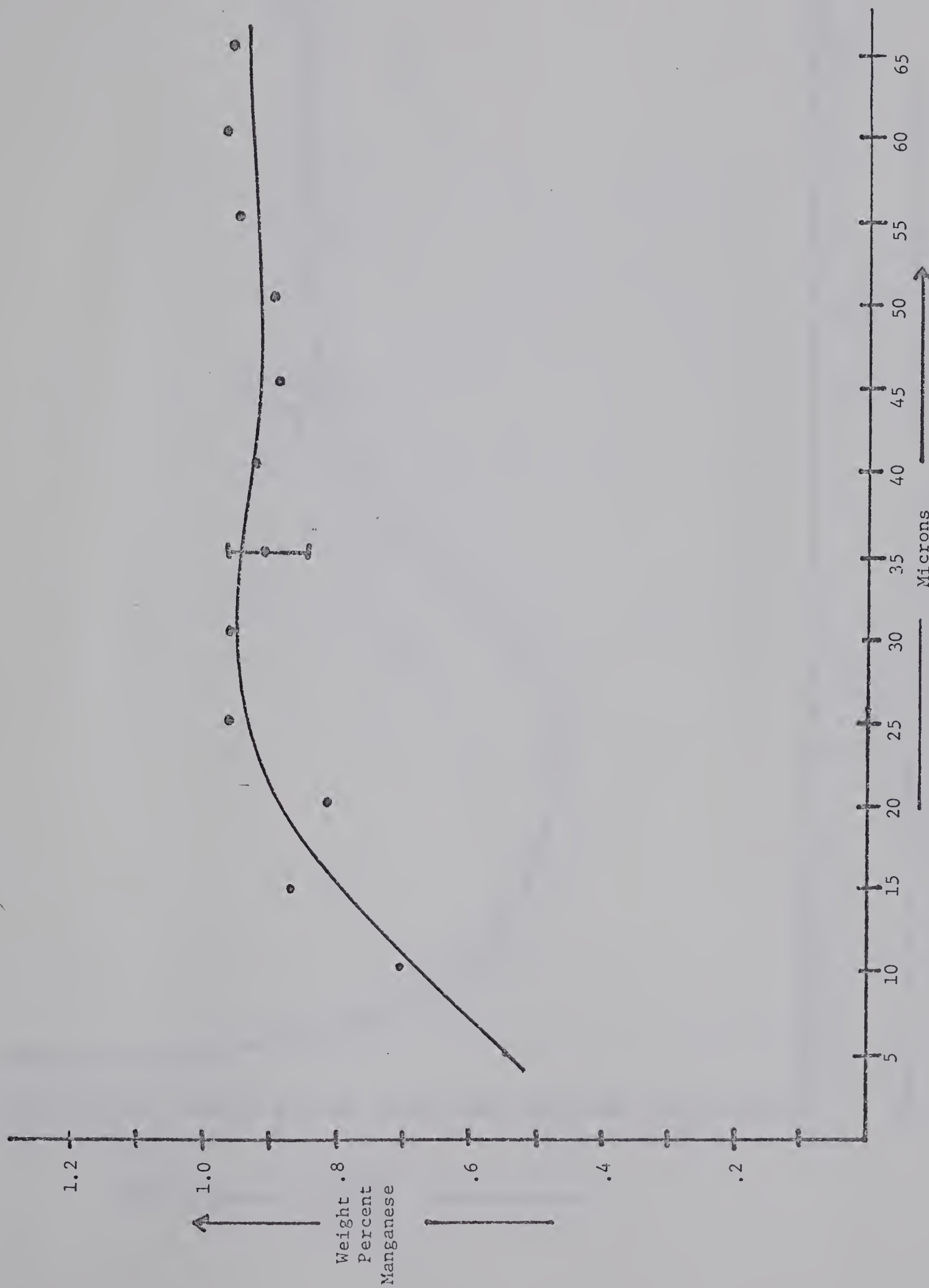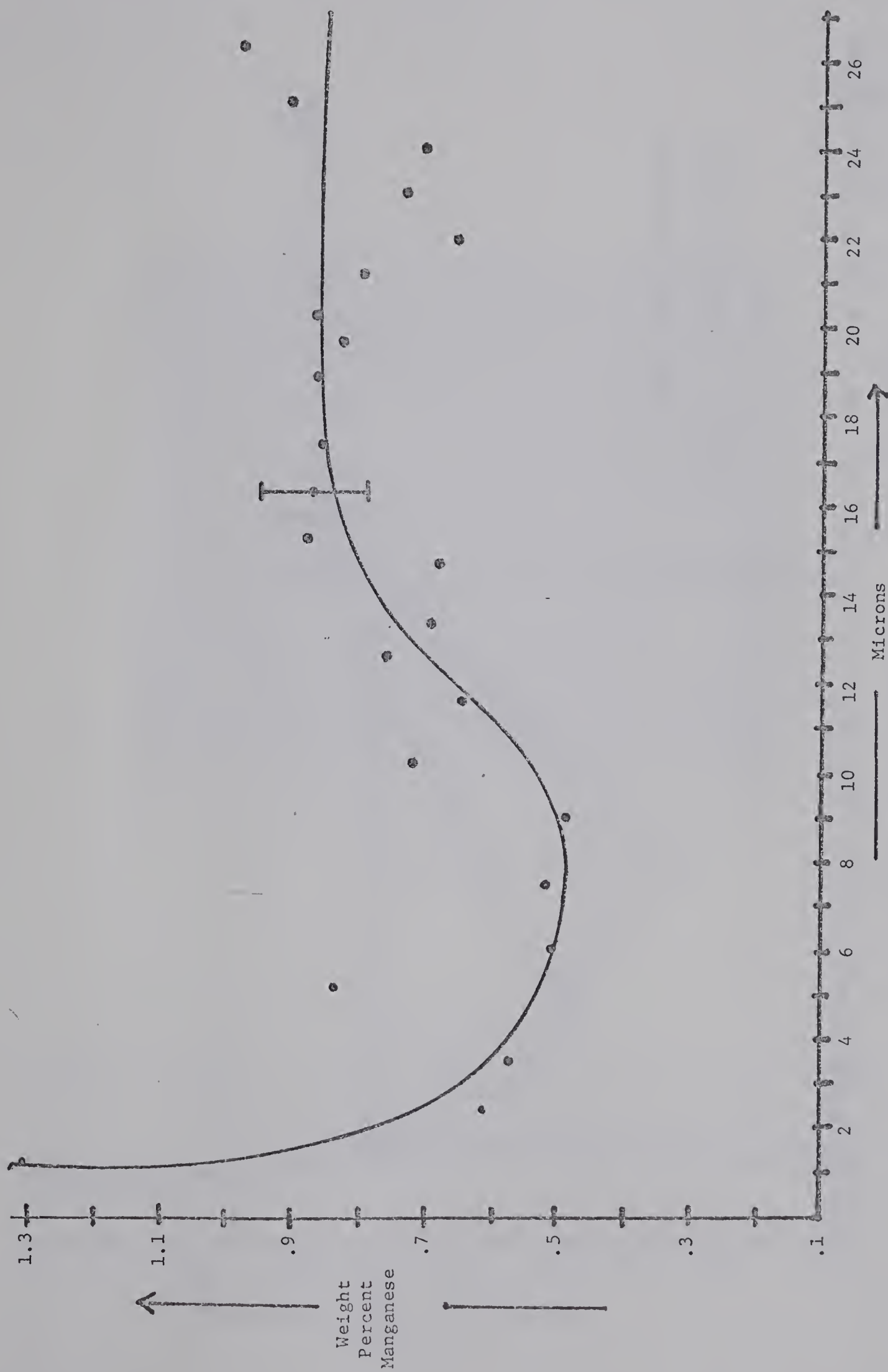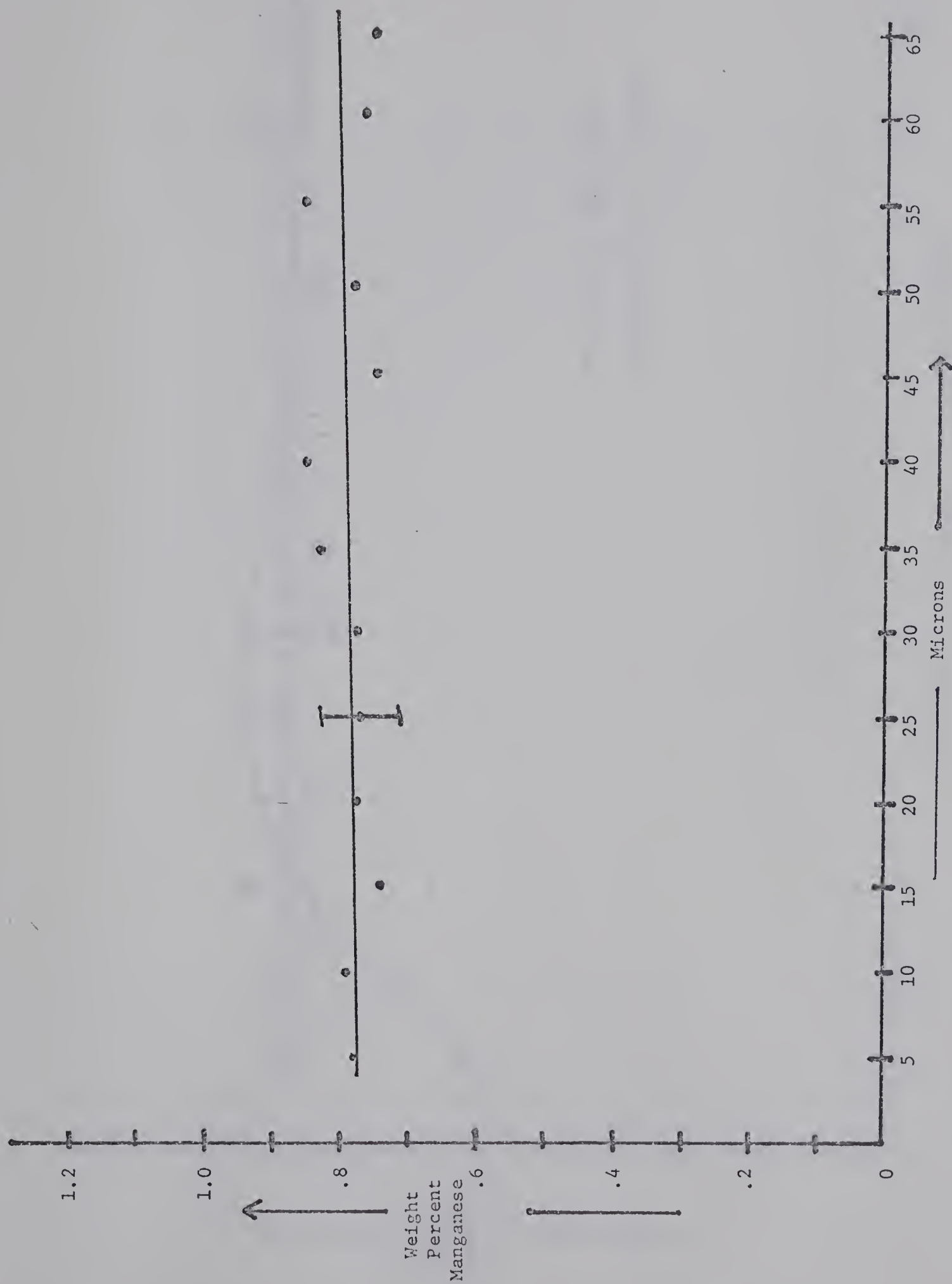
Figure 38. Variation in manganese concentration with depth below the free surface, determined with the electron microprobe, specimen 2-7.
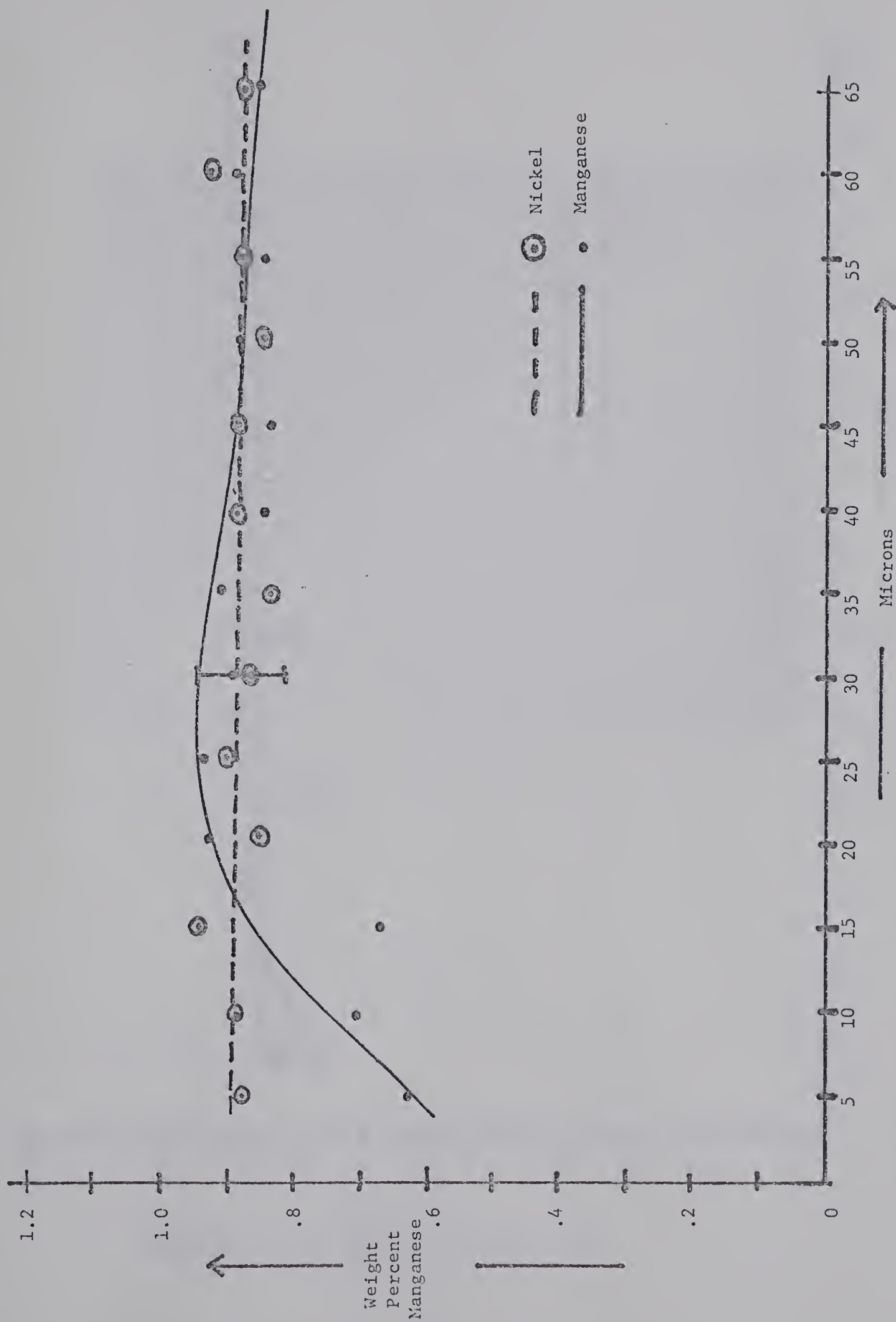
Figure 39. Variation in manganese and nickel concentration with depth below the free surface, determined with the electron microprobe, specimem 4-1.
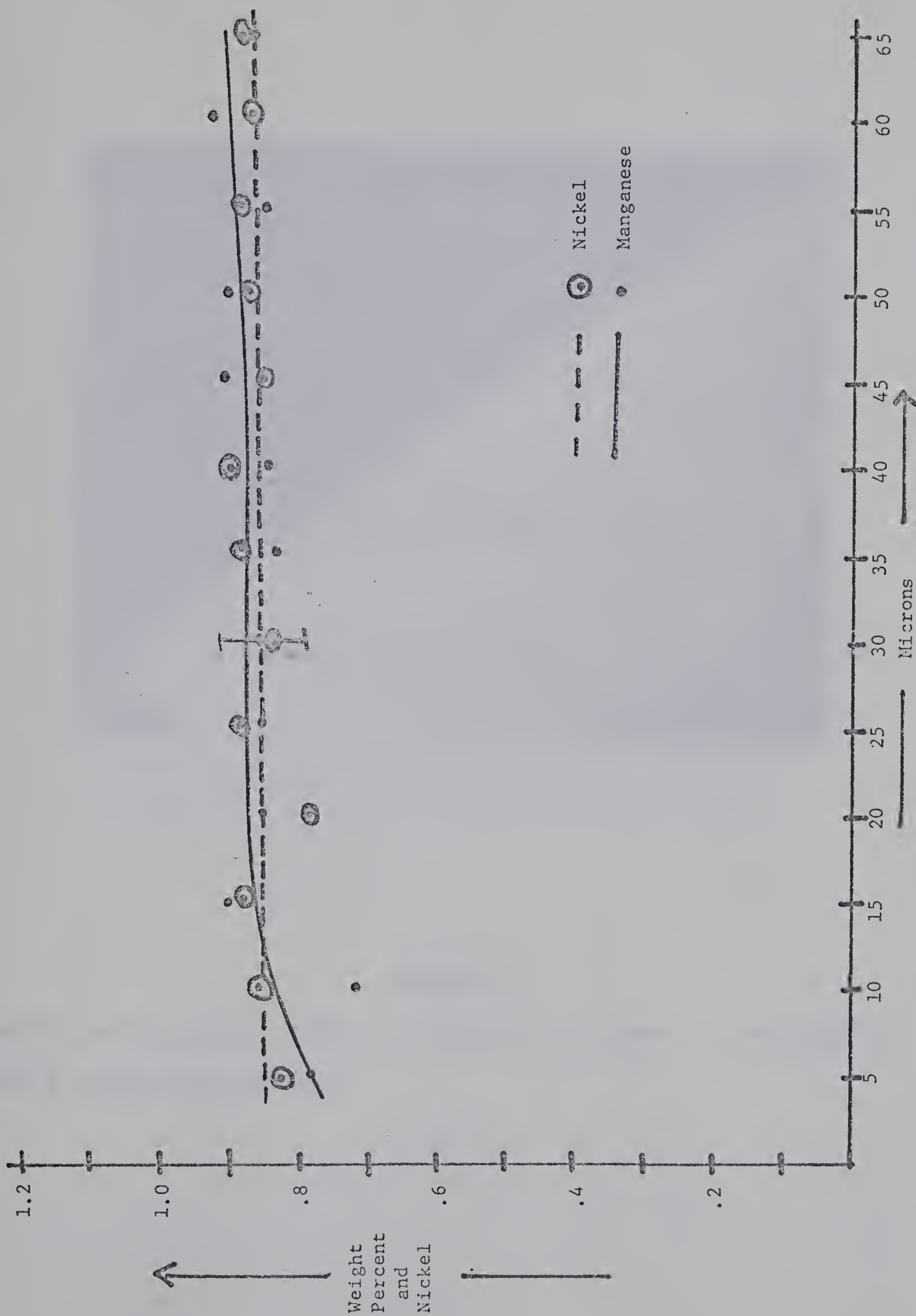
Figure 40. Variation in manganese and nickel concentration with depth below the free surface, determined with the electron microprobe, specimen 4-2.
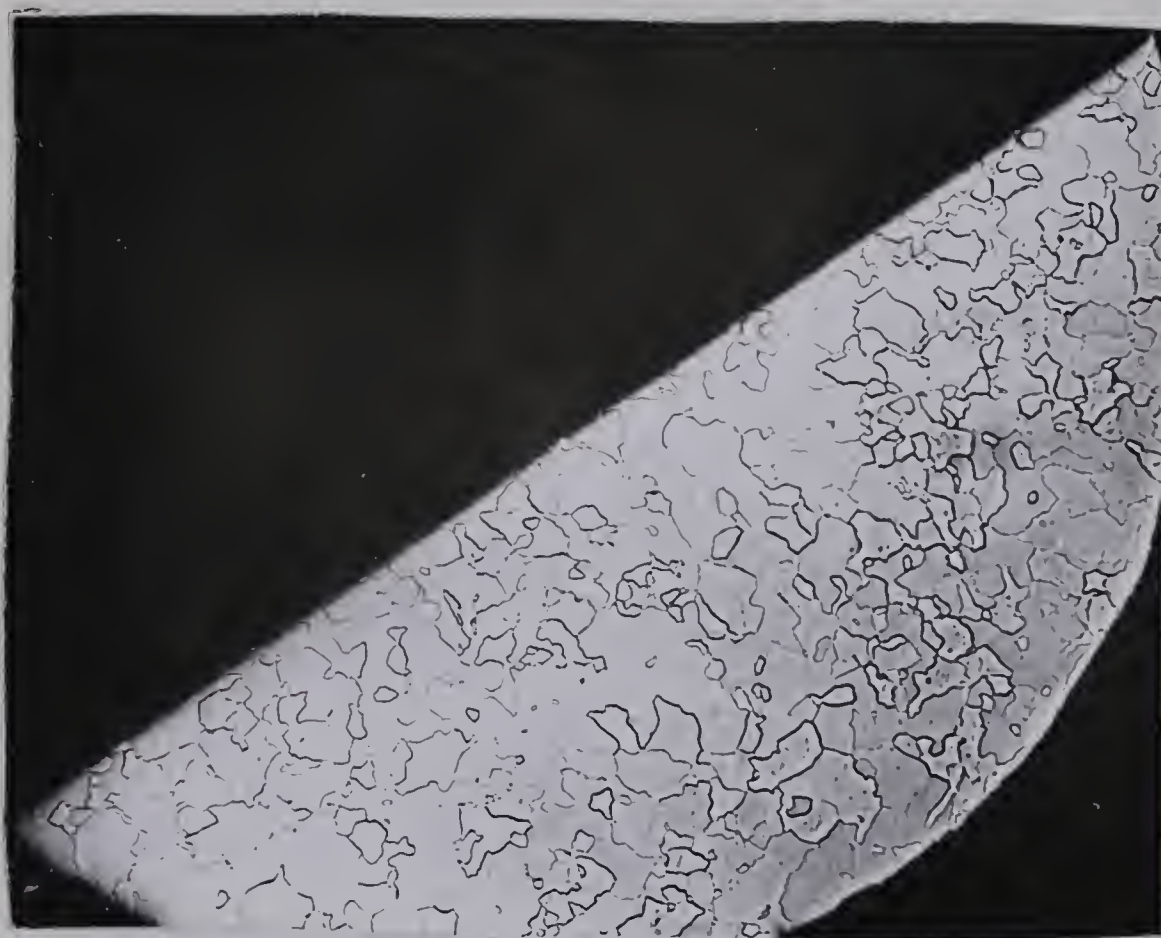
Figure 41

Optical micrograph of electron microprobe specimen 1-1, annealed at 1400°F. (Magnification x16).
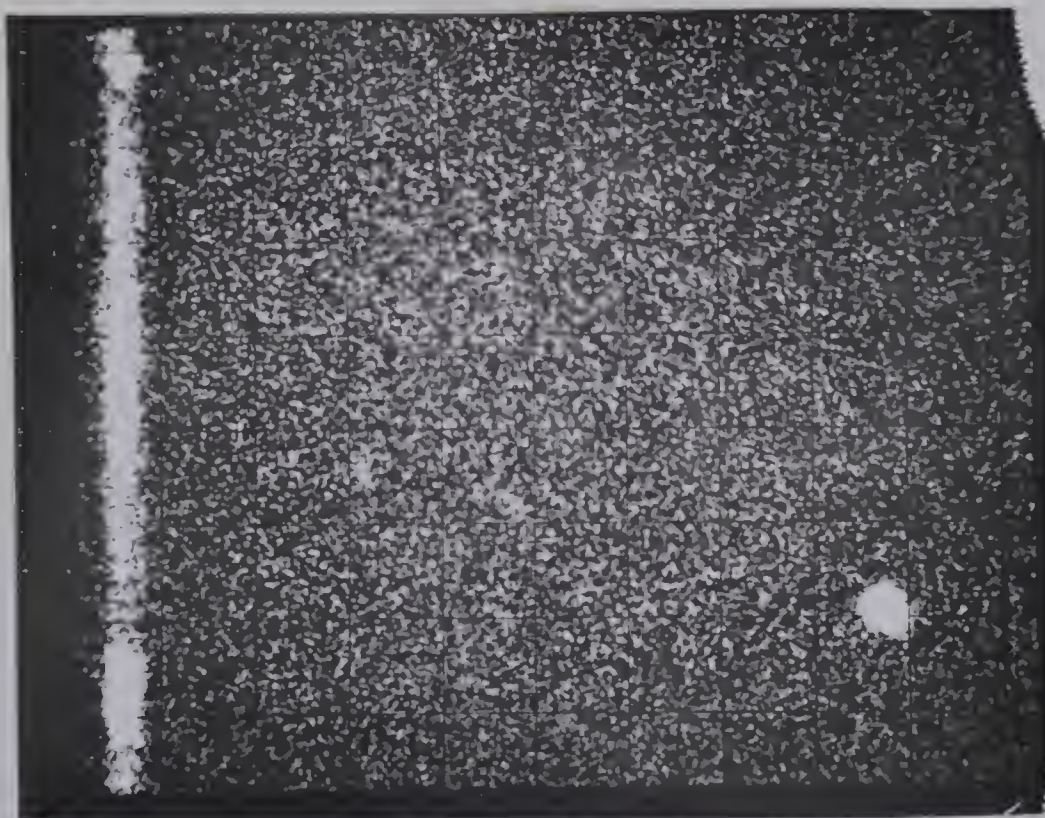
Specimen Holder
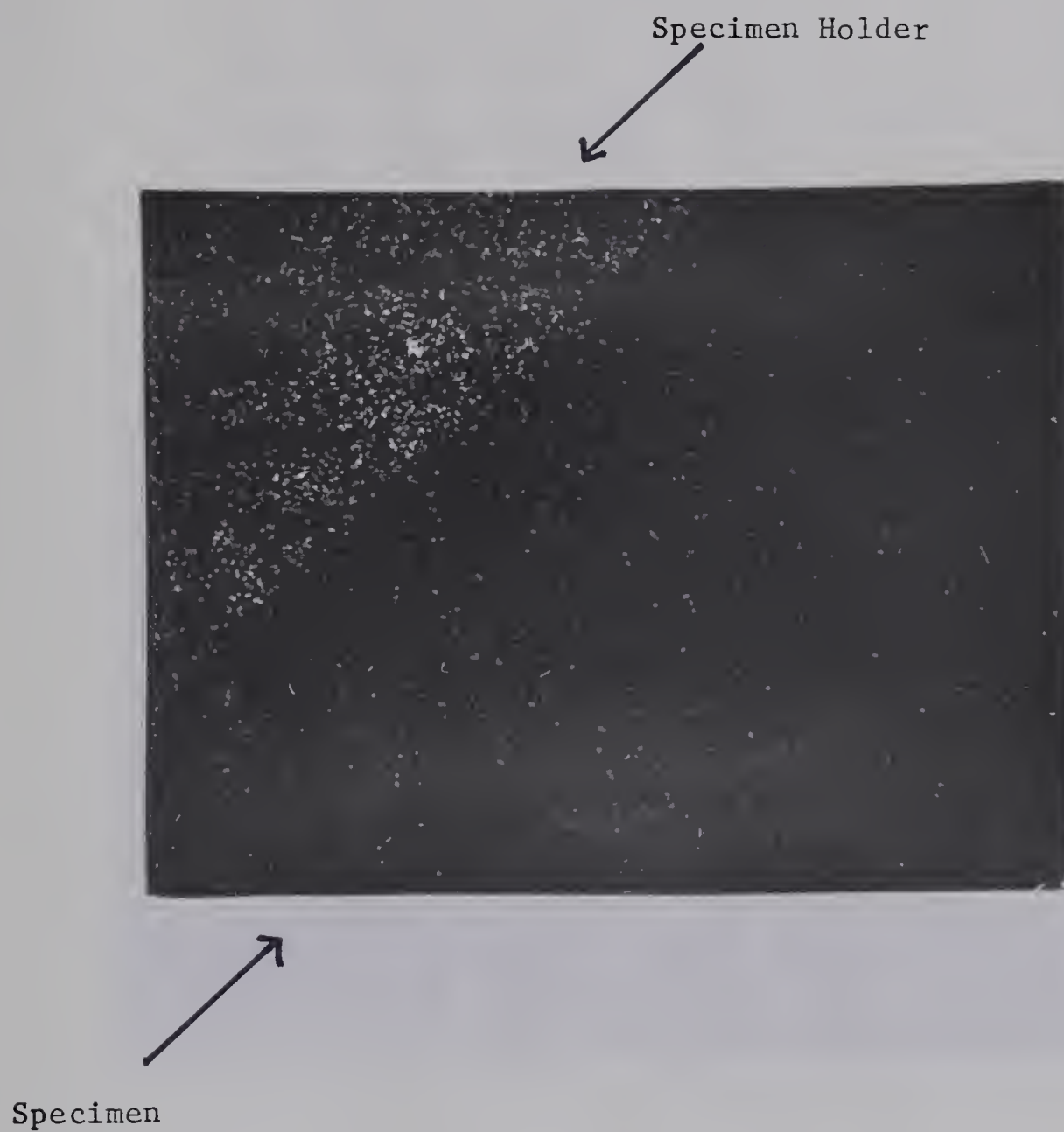
Specimen

Figure 42

Electron microprobe photograph of specimen 3B-2 showing the sulfur distribution resulting from an anneal at $1400^\circ F$. The long dimension of the photograph equals 150 microns.

Figure 43

Scanning electron microscope photograph of specimen 1-5, 2-1, 3A-2
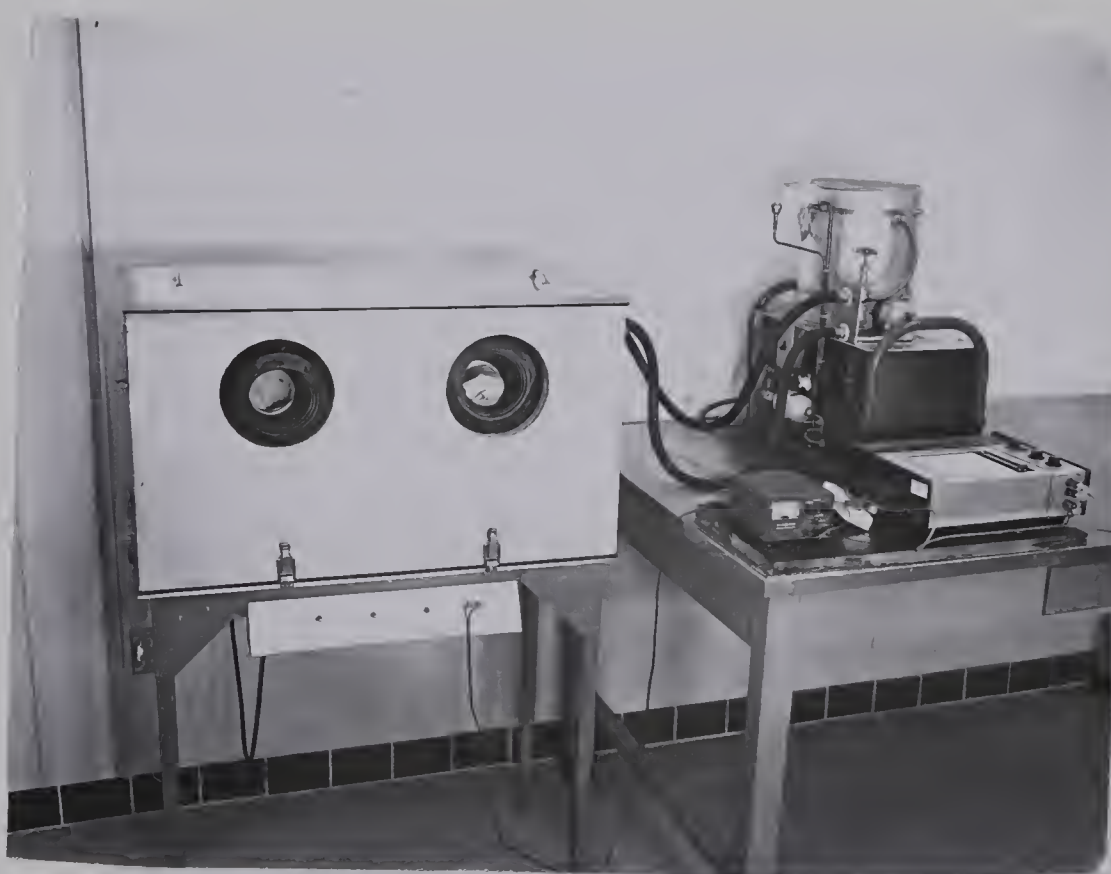
Figure 44

Photograph of electro-sectioning equipment.

Figure 45

Photograph of electro-sectioning equipment with the glove box removed.

Figure 46

Photograph of electro-sectioning equipment in simulated operation.

Appendices

Appendix 1

A Detailed Description of the Operation

of the Electro-Sectioning Equipment

Design

Figure 44 is a photograph of the electro-sectioning equipment and shows the refrigeration unit, strip chart recorder, voltage regulator and glove box. The coolant from the refrigeration unit (50% anti-freeze, 50% water) is pumped through copper tubing which runs just below the lucite cover of the glove box. Aluminum cooling fins are positioned on the tubing approximately 0.75 inches apart. All six inside surfaces of the glove box are covered with one inch thick styrofoam for insulation.

Figure 45 is a photograph of the equipment inside the glove box and shows the stainless steel electro-sectioning wheel and its drive system, a specimen and a specimen holder (top and bottom view) and the specimen drive system. On top of the specimen drive system is a swinging arm. It is possible to vary the pressure of the specimen upon the filter paper by varying the position of a weight along the arm.

Figure 15 is a schematic of the electrical design of the sectioning equipment.

Operating Conditions

This section will describe the operation of a typical electro-sectioning experiment.

Electro-Sectioning Procedure

First, two circular strips (8.25 inches O.D. and 6.0 inches I.D.) are removed from two pieces of filter paper (Watman's #50, Acid Resisting Filter Paper, 50 cm. in diameter) with the use of a scapel.

These strips are then placed on the sectioning wheel and a circular aluminum plate is placed on top of these strips to hold down the edges. The aluminum plate is fixed in position relative to the strips and the sectioning wheel (Figure 46). The sample is fixed in the specimen holder and placed on aluminum plate. All these operations are done with the glove box in position, operating through the top with the lucite cover removed. At this point the cover is placed in position and coolant is pumped through the tubing. While the temperature of the glove box slowly drops it is necessary to have the specimen drive in the position observed in Figure 45 and running. Approximately one hour is required to reach the operating temperature (4° to 8°C) for optimum polishing conditions. During this time, the electrolyte is prepared (765 ml. glacial acetic acid, 185 ml. perchloric acid and 50 ml. distilled water (12)), put into a squeeze bottle and left in a refrigerator. The squeeze bottle is placed in the glove box once the glove box reaches operating temperature. The temperature is controlled by the flow of coolant. The flow is shut off at 4°C and started up again at 8°C.

As soon as the temperature is between 4° and 8°C, the electro-sectioning can begin. The strip chart recorder begins recording voltage across the one ohm resistor and the electrolyte is squeezed onto the filter paper in front of the specimen. The required amount of electrolyte is that which will be completely absorbed by the filter paper and wet the surface of the sectioning wheel. If any less is applied the filter paper will not wet and stick to the wheel and if more is applied, material will be removed from the sides as well as the surface of the specimen. It is necessary to impregnate the filter paper up to the first black mark on the aluminum plate in front of the sample. It is

also necessary to have the division between impregnated and dry filter paper as sharp as possible. The specimen drive system is shut off, the sample placed in the drive system and then the system is turned on. Once the specimen is rotating (counter clockwise) evenly over the filter paper the drive mechanism of the wheel is also turned on. The sectioning wheel rotates counter clockwise beneath the specimen. Once the specimen reaches the first mark on the aluminum (the division between dry and impregnated filter paper) the voltage supply is increased from zero to eight volts in approximately fifteen seconds. This procedure correlates the position of the sample on the filter paper and the horizontal position of the pen on the strip chart.

If conditions are such that the surface of the specimen is being polished, the filter paper shows a light brownish stain as it passes from under the sample. This provides an excellent check. A dark brown stain indicates that polishing is occuring at a fast rate, while a light brown stain indicates a slower rate. The stain provides a good method of judging if the amount of electrolyte needs to be altered. To end the electro-sectioning the voltage regulator is turned off when the specimen is exactly opposite a black mark and the specimen is taken off the filter paper. The marks are placed one inch apart on the aluminum plate. By counting the number of marks the specimen passes and knowing there is a correlation between the position of the specimen in relation to the black marks and the horizontal position of the pen on the strip chart, it is possible to determine the total current that passed through the specimen between any two black marks. The total current determines the depth of material removed from the surface (Appendix 2).

The best polished specimen surface is produced when the sample is rotated at its slowest speed (about 1.66 revolutions/minute), the sectioning wheel at its fastest speed (about 0.95 revolutions/hour), and with the maximum pressure on the specimen. It was found that the voltage regulator supplied a constant eight volts and the strip chart measured 0.1 volts full scale.

Because the electrolyte evaporates readily it is only necessary to impregnate the filter paper several inches in front of the specimen. As the sectioning wheel revolves, intermittently electrolyte is added to the filter paper several inches in front of the specimen. In some cases the sectioning had to be terminated as a result of the filter paper forming humps, causing the specimen to topple out of the drive system. This was corrected by cutting the bottom piece of filter paper at a slightly greater diameter than the top piece. If the outside edges of the filter paper do not cross over, humping is eliminated.

Analysis of the Filter Paper

Once the sectioning is complete the specimen is taken off the filter paper, the coolant pump turned off and the temperature of the glove box allowed to increase. After approximately fifteen minutes the filter paper is dry. The filter paper is removed from the glove box and placed on a clean glass sheet. The aluminum plate is placed over the filter paper in the same relative position as during the sectioning. Starting with the first black mark (the division between dry and impregnated filter paper) one inch sections of filter paper are removed and placed in 50 ml. beakers. If twenty-four black marks are passed during the sectioning there will be twenty-four beakers with a one inch section of filter paper in each beaker.

To each beaker is added 10 to 15 ml. aqua-regia. Each beaker is heated and agitated until the filter paper dissolves. Filtration removes any undissolved filter paper. Following this operation the volume of each beaker is brought to 5 cm^3.

Atomic Absorption Spectrometry

For atomic absorption, standard solutions of 5, 10, 15 and 20 parts/million manganese and nickel are prepared. The atomic absorption readings are determined for each solution and each element. In each case, within the 0 to 20 ppm range, a straight line relationship was found between the atomic absorption readings and the concentration. Each 5 cm^3 solution is then analyzed for manganese or nickel. The concentration of solute is recorded. Calculations (Appendix 2) yield a plot of solute concentration against depth below the surface.

Maintenance

Since the electrolyte evaporates, exposed surfaces within the glove box readily corrode. Such surfaces, where possible, were sprayed with Glyptal, a protective electrical finish. After several runs the sectioning wheel becomes discolored. The wheel is removed and polished with 600 grit paper to remove the stains and produce a shiny surface.

Appendix 2

Calculations Involving the Electro-Sectioning Data

Definition of Terms

AS; ampere-seconds

P; parts/million

2.5; valence of iron

55.85; atomic weight of iron

7.86; density of iron.

Strip Chart Recorder

The current which flows through the specimen during electro-sectioning also runs through a one ohm resistor. The strip chart recorder measures the voltage across this resistor. The area under the curve is a measure of the total current which passes through the specimen. Because there is a correlation between the position of the specimen on the filter paper and the horizontal position of the pen on the strip chart, the amount of current that passes through the specimen between any two black marks on the aluminum plate can be determined. Assume that the number of ampere-seconds that passes through the specimen between any two black marks is AS. From Faraday's Law this represents a certain number of grams of material being removed, $AS = (AS)(55.85)/(96,500)(2.5)$ gm. This weight of iron represents a certain volume, $(AS)(55.85)/(96,500)(2.5)(7.86)$ cm^3. The surface area of the specimen exposed to electro-sectioning is 0.245π cm^2 (diameter approximately equals 0.99 cm). Thus the depth of material removed can be calculated and is $(AS)(55.85)/(96,500)(2.5)(7.86)(0.245\pi)$ cm. From the difference in specimen weight before and after a polish compared to the theoretical weight of material removed, an efficiency of 81% was found for the electro-sectioning

equipment. Therefore the depth of material removed by AS ampere-seconds

is (AS)(55.85)(0.81)/(96,500)(2.5)(7.86)(0.245π) cm. This is equal to

(AS)(0.31) microns. Each square inch of chart paper is equal to six

ampere-seconds and is therefore equivalent to removing (6)(0.31) = 1.86

microns from the sample surface. Thus, it is possible to determine

the depth of material removed from the specimen surface between every

pair of marks on the aluminum plate. The sum of the depths removed

between each set of marks is the total depth of material removed.

Filter Paper Analysis

The filter paper following an electro-sectioning experiment is

partitioned. The individual sections are dissolved in aqua regia and

analyzed by atomic absorption spectrometry. The solute concentration

(parts/million) is determined from a volume of 5 ml. A reading of

P parts/million solute in this solution is equivalent to

(P)/(1000)(200) = 5P x 10^{-6} gm. of solute. Since the depth of material

removed can be calculated and the area of the specimen is known, the

volume of material removed can be calculated. The mass of this volume

can be determined and is found to be (AS)(3.1 x 10^{-4})(0.245π)(7.86) gm.

Therefore the weight fraction of solute in each 5 cm^3 sample is

(5P x 10^{-6})/(AS)(3.1 x 10^{-5})(0.245)(7.86).

By analyzing each one inch section of filter paper for solute

concentration and determining the corresponding number of ampere-

seconds passing through the specimen, a graph of weight percent solute

against depth below the free surface is determined.

Appendix 3

Analysis of the Materials Used

Armco Ingot Iron, HP

	Maximum %	Typical %
carbon	.010	.003
manganese	.05	.02
phosphorous	.010	.003
sulfur	.005	.002
copper	.150	.078
nickel	.05	.02
chromium	.02	.006
columbium	.005	.002
vanadium	.010	.003
molybdenum	.020	.003
nitrogen	.005	.002
oxygen	.005	.001
silicon	.010	.002
cobalt	no max. specified	.003
bismuth	"	.000
silver	"	.0003
arsenic	"	.003
antimony	"	.001
zinc	"	.001
lead	"	.0003
tin	"	.001

This analysis was provided by the Armco Steel Corporation.

Manganese

Electrolytic manganese metal powder was obtained from Fisher Scientific Company. The assay from this supplier indicates the powder to be 99.94% pure, containing 0.003% iron.

Nickel

High purity nickel rods were provided by Falconbridge Nickel Mines Limited and the analysis is as follows.

Element	Concentration in Parts/Million
As	4
Ag	less than 0.4
Al	10
Ba	less than 8
Bi	less than 5
B	less than 50
C	100
Ca	less than 6
Cb	-
Cd	less than 25
Co	220
Cr	1
Cu	9
Fe	less than 20
Mg	2
Mo	less than 8
Na	-
P	-

Element	Concentration in Parts/Million
Pb	less than 20
S	3 to 8
Sb	-
Se	1
Si	less than 11
Sn	less than 25
Ta	-
Te	less than 1
Ti	less than 10
V	less than 8
W	-
Zn	less than 50
Zr	-
H_2	0.4
N_2	5
O_2	32

Element	Concentration in Parts/Million

Appendix 4

Physical Data (13), (20), (21)

	Manganese	Iron	Nickel
Atomic Number	25	26	28
Atomic Weight	54.94	55.85	58.71
Density (gm/cm^3)	7.2	7.86	8.9
Melting Point (^{o}C)	1244	1535	1455
Boiling Point (^{o}C)	2087	2800	2800
Electronic Configuration	$(-)(3d^5)(4s^2)$	$(-)(3d^6)(4s^2)$	$(-)(3d^8)(4s^2)$
Crystal Structure (1400°F)	complex cubic	bcc	fcc
Group	VII A	VIII A	VIII A
Distribution Coefficient in Iron	0.083		0.417
Activity Coefficient in Iron	1.30 - 1.38		0.66 - 0.67
DB/DA	15.6		5.7

$$k = \text{distribution coefficient} = \frac{\text{solute concentration in solid}}{\text{solute concentration in liquid}}$$

$$\gamma = \text{activity coefficient} = \frac{\text{activity of a component of a solution}}{\text{atom fraction of this component}}$$